

Sodium sulphate ameliorates hypercholesterolemia via the upregulation of *Cyp7a1* in hepatocytes and alleviates hepatic insulin resistance via the downregulation of *Trib3* in mice with high cholesterol diets

YANHONG YANG^{1*}, SIPING YU^{2,3*}, HEDONG RONG^{2,3*}, ZILI LEI^{2*}, CHANGYUAN YANG^{2,3*}, HUIJUAN WU^{2,3}, TIANLE ZHANG², FEI YANG^{2,3}, YA NIE^{2,3}, LEI CHEN², QING HU², QI SONG² and JIAO GUO²

¹School of Clinical Medicine, The First Affiliated Hospital of Guangdong Pharmaceutical University, Guangzhou, Guangdong 510080, P.R. China; ²Guangdong Metabolic Disease Research Center of Integrated Chinese and Western Medicine, Key Laboratory of Glucolipid Metabolic Disorder, Ministry of Education of China, Institute of Chinese Medicine, Guangdong Pharmaceutical University, Guangdong TCM Key Laboratory for Metabolic Diseases, Guangzhou, Guangdong 510006, P.R. China; ³School of Traditional Chinese Medicine, Guangdong Pharmaceutical University, Guangzhou Higher Education Mega Center, Guangzhou, Guangdong 510006, P.R. China

Received July 2, 2023; Accepted December 6, 2023

DOI: 10.3892/etm.2024.12650

Abstract. Amelioration of hypercholesterolemia is essential for the treatment of atherosclerotic cardiovascular disease. Sodium sulphate is the effective component of mirabilite, which has been used in traditional Chinese medicine for the treatment of various diseases. In the present study, C57BL/6 mice were fed with a high-cholesterol diet (HCD) for 7 weeks and were treated with sodium sulphate in the last three of those weeks. Sodium sulphate significantly reduced the total cholesterol level and the low-density lipoprotein cholesterol/high-density lipoprotein cholesterol ratio in the serum of mice fed the HCD. In addition, cytochrome P450 7a1 and 39a1 were significantly upregulated in the livers of mice treated with sodium sulphate. Furthermore, tribbles pseudokinase 3 expression was significantly increased in the livers of mice fed the HCD, but was significantly reduced by sodium sulphate treatment. In terms of the insulin signaling pathway, the ratio

of phosphorylated AKT to total AKT in the livers of mice fed the HCD was significantly lower compared with that of control mice fed a normal diet, but was significantly increased by sodium sulphate treatment. Sodium sulphate treatment also reduced the levels of fibroblast growth factor (FGF)15 in the ileum and inhibited the FGF15/FGF receptor 4-Klotho β /c-Jun N-terminal kinase/c-Jun signaling pathway in the livers of mice fed the HCD. In addition, sodium sulphate changed the composition of the gut microbiota of mice fed the HCD. In conclusion, sodium sulphate may mitigate hypercholesterolemia and hepatic insulin resistance in mice fed an HCD.

Introduction

Hypercholesterolemia is a well-established risk factor for atherosclerotic cardiovascular disease (ASCVD), and ASCVD is one of the leading causes of mortality worldwide (1). It was estimated by The World Health Organization that 17.9 million individuals died from cardiovascular disease in 2019, and 85% of these deaths were due to a heart attack or stroke (2). Previous studies have confirmed that high levels of total cholesterol (TC) and low-density lipoprotein cholesterol (LDL-C) in the serum of adult humans and atherosclerotic mice are associated with ASCVD (3,4). Therefore, the discovery and development of anti-hypercholesterolemic drugs is essential to medical science.

Sodium sulphate is the effective ingredient of mirabilite, which is a type of mineral used as a drug in traditional Chinese medicine (5,6). Mirabilite is also a purgative (7), although the mechanism of its laxative and diarrhea-inducing effects requires further exploration. It is known that the entry of excessive quantities of bile acids into the colon can cause diarrhea (8). Also, the absorption of bile acids in the terminal ileum and colon is essential to the enterohepatic circulation of bile acids (9), and resection of the terminal ileum can cause

Correspondence to: Professor Zili Lei or Professor Jiao Guo, Guangdong Metabolic Disease Research Center of Integrated Chinese and Western Medicine, Key Laboratory of Glucolipid Metabolic Disorder, Ministry of Education of China, Institute of Chinese Medicine, Guangdong Pharmaceutical University, Guangdong TCM Key Laboratory for Metabolic Diseases, 280 Wai-Huan-Dong Road, Guangzhou Higher Education Mega Center, Guangzhou, Guangdong 510006, P.R. China
E-mail: 3182683090@qq.com
E-mail: gyguoyz@163.com

*Contributed equally

Key words: hypercholesterolemia, sodium sulphate, gene expression, insulin resistance, metabolism

bile acid diarrhea (8,10). Studies have also confirmed that bile acid malabsorption causes diarrhea (10,11). However, it is unclear whether mirabilite increases the level of bile acids in the colon. Bile acids induce the expression of fibroblast growth factor (FGF)15/19 in enterocytes by stimulating the activation of farnesoid X receptor (FXR) in these cells (12). FGF15/19 is released into the blood and interacts with FGF receptor 4 (FGFR4) and Klotho β (KLB) on the surface of hepatocytes to downregulate the expression of the cytochrome P450 family 7 subfamily A member 1 (*Cyp7a1*) gene, which encodes the rate-limiting enzyme in bile acid synthesis (13-15). It is hypothesised that if mirabilite reduces the absorption of bile acids in the intestine, it may increase the conversion of cholesterol to bile acids via inhibition of the FGF15/19 signaling pathway in hepatocytes.

The gut microbiota has been confirmed to be key in regulating the health of the host, particularly with regard to glucose and lipid metabolism (16). Previous studies have reported that the gut microbiota also impacts the cholesterol and bile acid metabolism of the host (17,18). Gut microbial-derived metabolites, including short chain fatty acids, primary and secondary bile acids and trimethylamine N-oxide, have been found to have important functions in the maintenance of cardiovascular health (19). A recent study demonstrated that plant proteins can ameliorate hypercholesterolemia in hamsters by regulating the gut microbiota (20). However, it remains unclear if sodium sulphate regulates the metabolism of cholesterol and bile acids via modulation of the gut microbiota of the host.

In the present study, hypercholesterolemic mouse models were generated by feeding a high-cholesterol diet (HCD) to C57BL/6 mice. Three different doses of sodium sulphate were administered to the mice to study the efficiency of sodium sulphate as an anti-hypercholesterolemic agent and the underlying mechanisms.

Materials and methods

Mice. All mouse experimental procedures were approved by The Guangdong Pharmaceutical University Experimental Animal Ethics Committee (Guangzhou, China; approval no. gdpulacspf2017030-1) and are reported according to the ARRIVE guidelines. A total of 50 male C57BL/6 mice (age, 7 weeks; body weight, ~24 g) were purchased from Hunan Lex Jingda Laboratory Animal Co., Ltd. The mice were housed in a specific pathogen-free animal facility with a 12-h light/dark cycle and 60-65% humidity, at 25°C, and with free access to food and water. After 1 week of acclimatization, 40 mice were fed an HCD (Dyets, Inc.; cat. no. ASHF3; containing 22.60% protein, 45.20% carbohydrate, 20.10% fat and 1.25% cholesterol) and the remaining 10 mice continued to be fed a normal food diet (NFD; Beijing Keao Xieli Feed Co., Ltd.; cat. no. 2212; containing 23.07% protein, 65.08% carbohydrate and 11.85% fat). After 4 weeks, the mice fed the HCD were divided into four groups (n=10/group), based on the TC concentration observed in the serum from blood collected from the tail vein, such that the TC level was similar in each group (Fig. S1A and B). The dosage of sodium sulphate used in the present study was based on the sodium sulphate content in mirabilite administered to mice and rats in a previous study (6). In three of the HCD groups, mice were intragastrically

treated with sodium sulphate (Damao Chemical Regent Factory; cat. no. 7757-82-6) at a low dose (LSS; 158.5 mg/kg/day; aqueous solute, 0.01 ml/g/mouse), middle dose (MSS; 317.0 mg/kg/day; aqueous solute, 0.01 ml/g/mouse) and high dose (HSS; 634.0 mg/kg/day; aqueous solute, 0.01 ml/g/mouse), along with the HCD. As such, these three groups were designated the HCD + LSS, HCD + MSS and HCD + HSS groups, respectively. The fourth HCD group was fed the HCD only and was designated the HCD group. The mice fed the NFD were used as the control group (CON group). Mice from the CON and HCD groups were intragastrically administered an equal volume of water (0.01 ml/g/mouse). The body weight of the mice was measured once a week. After 3 weeks of sodium sulphate administration, blood was collected from the orbital vein of the mice following anesthesia with 3% isoflurane. After blood collection, the mice were sacrificed via cervical dislocation. Animal death was confirmed through the stoppage of breathing. The hepatic tissues and intestines of the mice were then collected for biochemical, histological and molecular analyses.

Blood and hepatic biochemical profile assays. The concentrations of TC and triglycerides (TG) in the serum and hepatic tissues, and the concentrations of high-density lipoprotein cholesterol (HDL-C), LDL-C, total bile acid (TBA), alanine aminotransferase (ALT) and aspartate aminotransferase (AST) in the serum were measured according to the manufacturer's protocols for each kit. The kits for measuring the concentrations of TC (cat. no. A111-1-1), TG (cat. no. A110-1-1), HDL-C (cat. no. A112-1-1), LDL-C (cat. no. A113-1-1), TBA (cat. no. E003-2-1), ALT (cat. no. C009-2-1) and AST (cat. no. C010-2-1) were purchased from Nanjing Jiancheng Bioengineering Institute.

Haematoxylin and eosin (H&E) staining. Mouse hepatic tissues were fixed in 4% paraformaldehyde at 4°C overnight and then embedded in paraffin for H&E staining. The 4- μ m paraffin sections were stained with haematoxylin (cat. no. H9627; Sigma-Aldrich; Merck KGaA) for 3 min followed by eosin (cat. no. E4009; Sigma-Aldrich; Merck KGaA) for 20 sec, both at room temperature. The images were captured with a PerkinElmer Automated Quantitative Pathology System (PerkinElmer, Inc.).

Transcriptome analysis. Hepatic tissues from each group of mice were fresh frozen in liquid nitrogen and then stored at -80°C. RNA extraction, library construction, sequencing and transcriptome analysis were all conducted by Guangzhou Gene Denovo Biotechnology Co., Ltd. Briefly, total RNA from each sample was extracted using TRIzol[®] reagent (Invitrogen; Thermo Fisher Scientific, Inc.). The RNA quality was evaluated using an Agilent 2100 Bioanalyzer (Agilent Technologies, Inc.) and then checked via RNase-free agarose gel electrophoresis. Following extraction, eukaryotic mRNA was enriched using oligo(dT) beads (New England BioLabs, Inc.). The enriched mRNA molecules were fragmented in fragmentation buffer, and then reverse transcribed into cDNA using random primers (New England BioLabs, Inc.). The cDNA fragments were subsequently purified using a QiaQuick PCR extraction kit (Qiagen China Co., Ltd.), followed by end-repaired

poly(A) addition and then ligation to Illumina sequencing adapters. The HiSeq Rapid Cluster Kit v2 (PE-402-4002) and HiSeq Rapid SBS Kit v2 (FC-402-4023) were used. The ligation products were separated by size via agarose gel electrophoresis, then PCR amplified and finally sequenced using an Illumina HiSeq 2500 System (Illumina, Inc.). Then, an ABI StepOnePlus Real Time PCR System (hermo Fisher Scientific, Inc.) was used to detect library concentration. The concentration was $>5 \text{ ng}/\mu\text{l}$. The reads were then filtered using fastp (version 0.18.0) (21) and differential expression analysis was performed using DESeq2 software (version 1.20.0) (22). Differentially expressed mRNAs with a false discovery rate (FDR) <0.05 and absolute fold change ≥ 2 were considered included in subsequent analyses.

Kyoto Encyclopedia of Genes and Genomes (KEGG) is a public pathway-related database used to analyze identified significantly enriched metabolic pathways or signal transduction pathways of differentially expressed genes (DEGs) compared with the whole genome background (23). The calculated P-values underwent FDR correction, and KEGG pathways with FDR ≤ 0.05 were defined as significantly enriched pathways of the DEGs.

Reverse transcription-quantitative PCR (RT-qPCR). Total RNA was extracted from each hepatic tissue and ileal sample harvested from the experimental mice using TRIzol reagent, and then subjected to RT using the PrimeScript™ RT Reagent kit (Takara Bio, Inc.) at 37°C for 15 min followed by 85°C for 5 sec. qPCR was performed using the SYBR Premix Ex Taq kit (Takara Bio, Inc.) and the LightCycler 480II System (Roche Diagnostics). The thermocycling conditions were as follows: 95°C for 30 sec; and then 40 cycles of 95°C for 5 sec, 60°C for 20 sec and 65°C for 15 sec. GAPDH was used as the internal reference. All primers used for qPCR in the present study are listed in Table SI. The $2^{-\Delta\Delta C_t}$ method was used to quantify the relative transcriptional level of each gene (24).

Western blotting. Hepatic tissues were lysed in Radio-Immunoprecipitation Assay lysis buffer (Dalian Meilun Biology Technology Co., Ltd.), and then centrifuged at 13,680 x g at 4°C for 30 min to harvest the supernatant. The protein concentration in the supernatant was measured using a BCA kit (cat. no. P0011; Beyotime Institute of Biotechnology). Then, equal amounts of protein (32 $\mu\text{g}/\text{lane}$) were separated using SDS-PAGE (10% gel) and subsequently transferred to a PVDF membrane. The PVDF membrane was blocked with 5% skimmed milk in Tris-buffered saline Tween 20 (0.1%) buffer for 1 h at room temperature, then incubated with primary antibodies at 4°C overnight. The primary antibodies comprised: Rabbit anti-GAPDH (1:1,000; cat. no. 2118S; CST Biological Reagents Co., Ltd.), mouse anti-CYP7A1 (1:1,000; cat. no. 2683295; MilliporeSigma), rabbit anti-hydroxy- δ -5-steroid dehydrogenase, 3 β - and steroid δ -isomerase 7 (HSD3B7; 1:1,000; cat. no. ab190223; Abcam), rabbit anti-aldo-keto reductase family 1 member D1 (AKRID1; 1:1,000; cat. no. ab101393; Abcam), rabbit anti-acyl-CoA oxidase 2 (1:1,000; cat. no. ab197808; Abcam), rabbit anti-hydroxysteroid 17- β dehydrogenase 4 (HSD17B4; 1:1,000; cat. no. ab97971; Abcam), rabbit anti-CYP27A1 (1:2,000; cat. no. ab126785; Abcam), rabbit anti-CYP39A1 (1:1,000;

cat. no. ab129334; Abcam), rabbit anti-isopentenyl-diphosphate δ isomerase 1 (IDI1; 1:3,000; cat. no. ab97448; Abcam), rabbit anti-lanosterol synthase [anti-oxidosqualene-lanosterol cyclase (OSC); 1:1,000; cat. no. ab80364; Abcam], rabbit anti-farnesyl diphosphate farnesyltransferase 1 (FDFT1; 1:1,000; cat. no. ab195046; Abcam), rabbit anti-farnesyl diphosphate synthase (FDPS; 1:2,000; cat. no. ab153805; Abcam), rabbit anti-mevalonate diphosphate decarboxylase (MVD; 1:1,000; cat. no. ab96226; Abcam), rabbit anti-mevalonate kinase (MVK; 1:1,000; cat. no. ab154515; Abcam), rabbit anti-3-hydroxy-3-methylglutaryl-CoA reductase (HMGCR; 1:1,000; cat. no. ab174830; Abcam), rabbit anti-low density lipoprotein receptor (LDLR; 1:1,000; cat. no. ab52818; Abcam), rabbit anti-c-Jun N-terminal kinase (JNK; 1:1,000; cat. no. 9252s; CST Biological Reagents Co., Ltd.), mouse anti-phosphorylated (p)-JNK (1:2,000; cat. no. 9255s; CST Biological Reagents Co., Ltd.), rabbit anti-p-insulin receptor substrate 1 (p-IRS1; Tyr608) mouse (1:1,000; cat. no. 09-432; MilliporeSigma), rabbit anti-IRS-1 (1:1,000; cat. no. 2382S; CST Biological Reagents Co., Ltd.), rabbit anti-p-AKT (Ser473) (1:1,000; cat. no. 4060S; CST Biological Reagents Co., Ltd.), rabbit anti-AKT (1:1,000; cat. no. 4685S; CST Biological Reagents Co., Ltd.), mouse anti-tribbles pseudokinase 3 (TRB3; 1:100; cat. no. sc-390242; Santa Cruz Biotechnology, Inc.), rabbit anti-c-Jun (1:1,000; cat. no. ab32137; Abcam), mouse anti-p-c-Jun (1:200; cat. no. sc-822; Santa Cruz Biotechnology, Inc.) and goat anti-KLB (0.5 $\mu\text{g}/\text{ml}$; cat. no. AF5889; R&D Systems China Co., Ltd.). Then, the PVDF membrane was washed in Tris-buffered saline Tween 20 (0.1%) buffer for 1 h at room temperature and subsequently incubated with horseradish peroxidase (HRP)-labeled secondary antibodies, including HRP-goat anti-rabbit IgG (1:5,000; cat. no. os0701; Earthox Life Sciences), HRP-donkey anti-goat IgG (1:2,000; cat. no. ab6885; Abcam) and HRP-goat anti-mouse IgG (1:2,000; cat. no. ab6789; Abcam) at room temperature for 1 h. Finally, the signals were detected using Enhanced Chemiluminescence ECL solution (cat. no. MA0186-2; Meilunbio), and quantification of the bands was conducted using ImageJ software (version 1.53a; National Institutes of Health).

16S ribosomal (r)DNA gene analysis. Fecal samples collected the day before tissue harvesting were flash frozen in liquid nitrogen after collection from each mouse and stored at -80°C until use. The extraction of bacterial DNA from the fecal samples, the PCR amplification of bacterial 16S rDNA genes, sequencing and analysis were conducted by Guangzhou Gene Denovo Biotechnology Co., Ltd. All experimental procedures were performed as previously described (25).

Statistical analysis. Statistical differences were determined using SPSS software (version 23.0; IBM Corp.). Data are presented as the mean \pm SEM. One-way ANOVA followed by Tukey's post hoc test was conducted to analyze differences among the groups. $P < 0.05$ was considered to indicate a statistically significant difference.

Results

Sodium sulphate ameliorates hypercholesterolemia in mice fed an HCD. To evaluate the effects of sodium sulphate on

hypercholesterolemia, 8-week-old male C57BL/6 mice were fed an HCD for 4 weeks, and then the TC concentration in the mice serum was determined (Fig. S1A). After 4 weeks of feeding with the HCD, the serum TC concentration was significantly higher compared with that of the mice in the CON group (Fig. S1B). The mice fed an HCD were then divided into four groups, with matching of the serum TC concentration in each group. Then, mice in the HCD + LSS, HCD + MSS and HCD + HSS groups were treated with sodium sulphate for 3 weeks (Fig. S1A). The body weight and food intake of mice in the CON, HCD, HCD + LSS, HCD + MSS and HCD + HSS groups exhibited no significant differences during these 3 weeks (Fig. S1C and D). Although the average daily defecation mass of mice fed an HCD was lower than that of the CON group, it was higher in the sodium sulphate treated mice compared with the CON and HCD groups (Fig. S1E). However, these differences in defecation mass were not found to be significant, and the fecal pellets of the mice in the sodium sulphate groups were normal.

Although the serum TC concentration of the mice in the HCD group was significantly higher than that in the CON group, administration of sodium sulphate significantly reduced the serum TC concentration in mice fed an HCD (Fig. 1A). However, the serum TG concentration of the mice in each group was similar (Fig. 1B). The TC level in the liver was significantly increased in the mice from the HCD group compared with the CON group (Fig. 1C). In addition, the TC level in the liver exhibited a downward trend in the mice from the HCD + LSS, HCD + MSS and HCD + HSS groups compared with the HCD group, but this reduction was not significant (Fig. 1C). The TG level in the liver was significantly higher in mice fed an HCD compared with those fed an NFD, and the administration of sodium sulphate did not reduce it (Fig. 1D). The serum LDL-C concentration did not significantly differ among the mice of the five groups (Fig. 1E). However, the serum HDL-C concentrations in the mice from the HCD + LSS, HCD + MSS and HCD + HSS groups were significantly higher than those in the mice from the HCD group (Fig. 1F). In addition, the LDL-C/HDL-C ratio was significantly reduced in the serum of the mice from the HCD + LSS and HCD + HSS groups compared with the HCD group (Fig. 1G). The serum TBA concentration in the mice from the HCD group was significantly reduced compared that in the mice from the CON group, and the serum TBA concentrations in the HCD + LSS, HCD + MSS and HCD + HSS groups were slightly but not significantly lower than the serum TBA concentration in the HCD group (Fig. 1H). In addition, when the serum ALT and AST concentrations were compared among the mice in all groups, no significant differences were detected (Fig. 1I and J). These results indicate that sodium sulphate may ameliorate the hypercholesterolemia in mice induced by an HCD.

Since the liver is the major organ involved in cholesterol metabolism (26), the morphology and histology of the livers of the mice in the five groups were assessed. The morphology of the livers in mice fed with an HCD with or without sodium sulphate appeared slightly paler compared with those in the CON group (Fig. S2A). The gallbladders from mice in the HCD group were dark red, and the administration of sodium sulphate improved the colour and increased the size of the gallbladders from these mice (Fig. S2A). The liver weight of

mice in the HCD group was significantly reduced compared with that in the CON group, although the reduction was slight, and the liver weights of mice in the sodium sulphate administration groups exhibited no significant differences compared with the HCD group (Fig. S2B). The liver/body weight ratio of mice fed an HCD was significantly lower than that of mice fed an NCD, and the administration of sodium sulphate did not increase the liver/body weight ratio of these mice (Fig. S2C). The results of H&E staining demonstrated that excessive quantities of lipid droplets accumulated in the liver tissues of mice from the HCD group, and the haematoxylin staining intensity of the nuclei in certain hepatocytes of this group was weaker (Fig. S2D). The weak nuclear staining indicated that the hepatocytes were damaged (27). Following the administration of sodium sulphate to mice fed an HCD, excessive lipid accumulation was still detected in the hepatocytes, but the nuclear staining in most hepatocytes of these mice was normal (Fig. S2D). These results demonstrated that, although sodium sulphate did not mitigate non-alcoholic fatty liver disease (NAFLD) in mice fed an HCD, it protected hepatocytes against HCD-induced damage.

Sodium sulphate upregulates the hepatic expression of bile acid synthesis-associated genes in mice fed an HCD. RNA-sequencing (seq) technology was used to compare the transcriptional profiles of hepatic tissues from mice in the CON, HCD and HCD + MSS groups. There were 148 upregulated and 230 downregulated genes in the hepatic tissues from the HCD group compared with the CON group (Fig. S3A and B). The mRNA expression levels of 116 genes were significantly increased and those of 127 genes were significantly decreased in the hepatic tissues from the HCD + MSS group compared with the HCD group (Fig. S3A and C). The expression levels of 203 genes were higher and those of 286 genes were lower in the hepatic tissues from the HCD + MSS group compared with the CON group (Fig. S3A and D). The RNA-seq results demonstrated that genes associated with bile acid synthesis, such as *Cyp7a1*, were upregulated in the livers of the HCD + MSS group compared with the HCD group (Fig. 2A). Since bile acid transporters play important roles in the regulation of bile acid metabolism (28), the transcriptional levels of genes encoding bile acid transporters in the liver were also analysed. The RNA-seq results demonstrated that the mRNA level of solute carrier organic anion transporter family member 1b2 (*Slco1b2*) was notably reduced in the hepatic tissues from the HCD group compared with the CON group, but there was no significant change in *Slco1b2* in the HCD + MSS group compared with the HCD group (Fig. S3E).

The expression levels of genes associated with bile acid synthesis were further tested via RT-qPCR and western blotting. *Cyp7a1* expression was increased at the mRNA level in the hepatic tissues from the HCD group compared with the CON group (Fig. 2B). However, the CYP7A1 protein expression level was slightly lower in the livers from the HCD group compared with the CON group, although this reduction was not significant (Fig. 2C and D). The *Cyp7a1* mRNA levels were significantly higher in the livers from the HCD + MSS and HCD + HSS groups compared with the HCD group (Fig. 2B), and the CYP7A1 protein levels were significantly increased in the liver tissues from the HCD + LSS and HCD + MSS groups

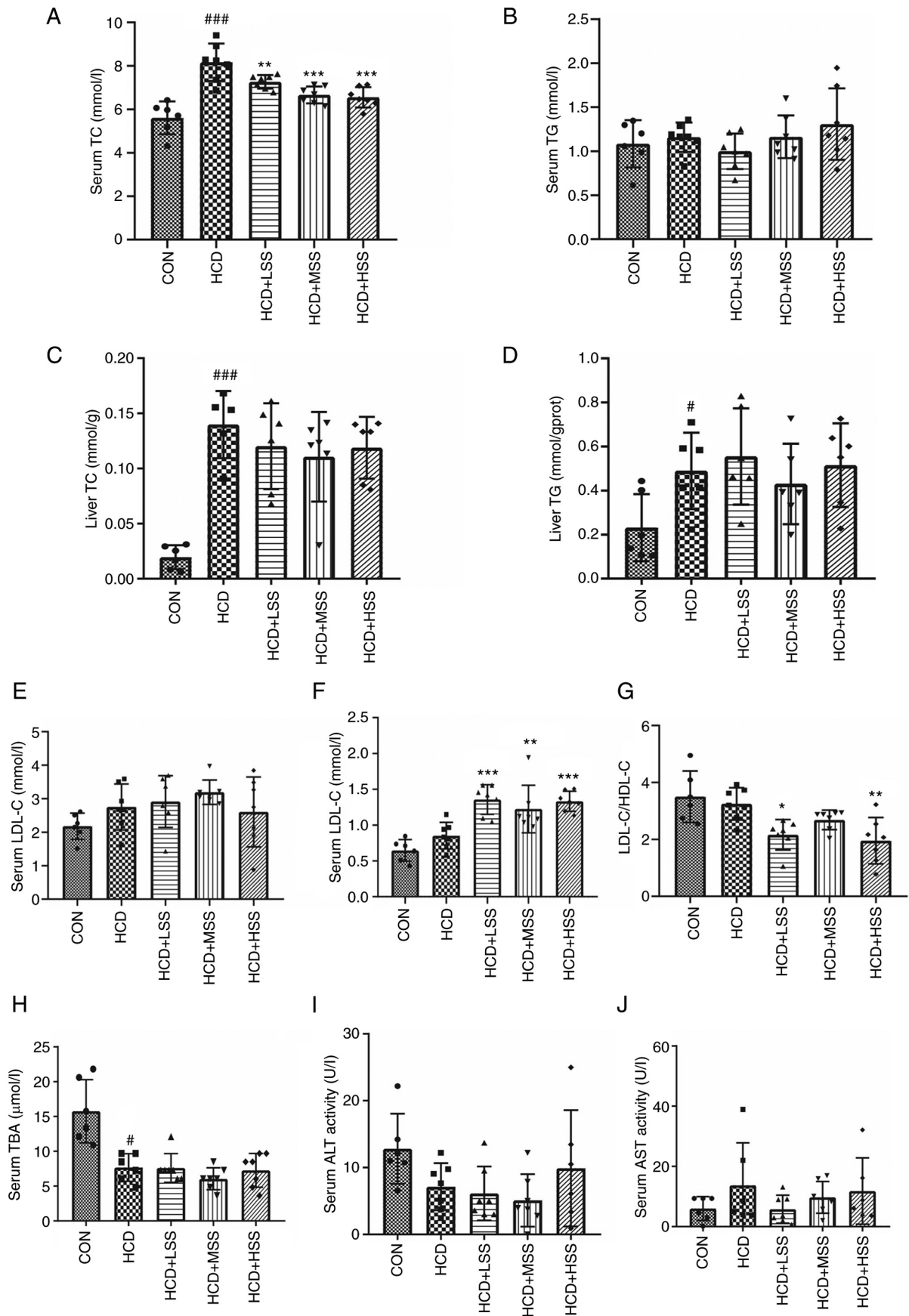


Figure 1. Effects of sodium sulphate on mice fed an HCD. Serum concentrations of (A) TC and (B) TG in mice from the five study groups: CON, HCD, HCD + LSS, HCD + MSS and HCD + HSS. Levels of (C) TC and (D) TG in the livers of the mice. (E) LDL-C concentration, (F) HDL-C concentration and (G) LDL-C/HDL-C ratio in the serum of the mice. Serum concentrations of (H) TBA, (I) ALT and (J) AST in the mice. **P*<0.05, ****P*<0.001 vs. the CON group; #*P*<0.05, ***P*<0.01, ****P*<0.001 vs. the HCD group. HCD, high cholesterol diet; TC, total cholesterol; TG, triglycerides; CON, control; LSS, low dose of sodium sulphate; MSS, middle dose of sodium sulphate; HSS, high dose of sodium sulphate; LDL-C, low-density lipoprotein cholesterol; HDL-C, high-density lipoprotein cholesterol; TBA, total bile acid; ALT, alanine aminotransferase; AST, aspartate aminotransferase; gprot, g of protein.

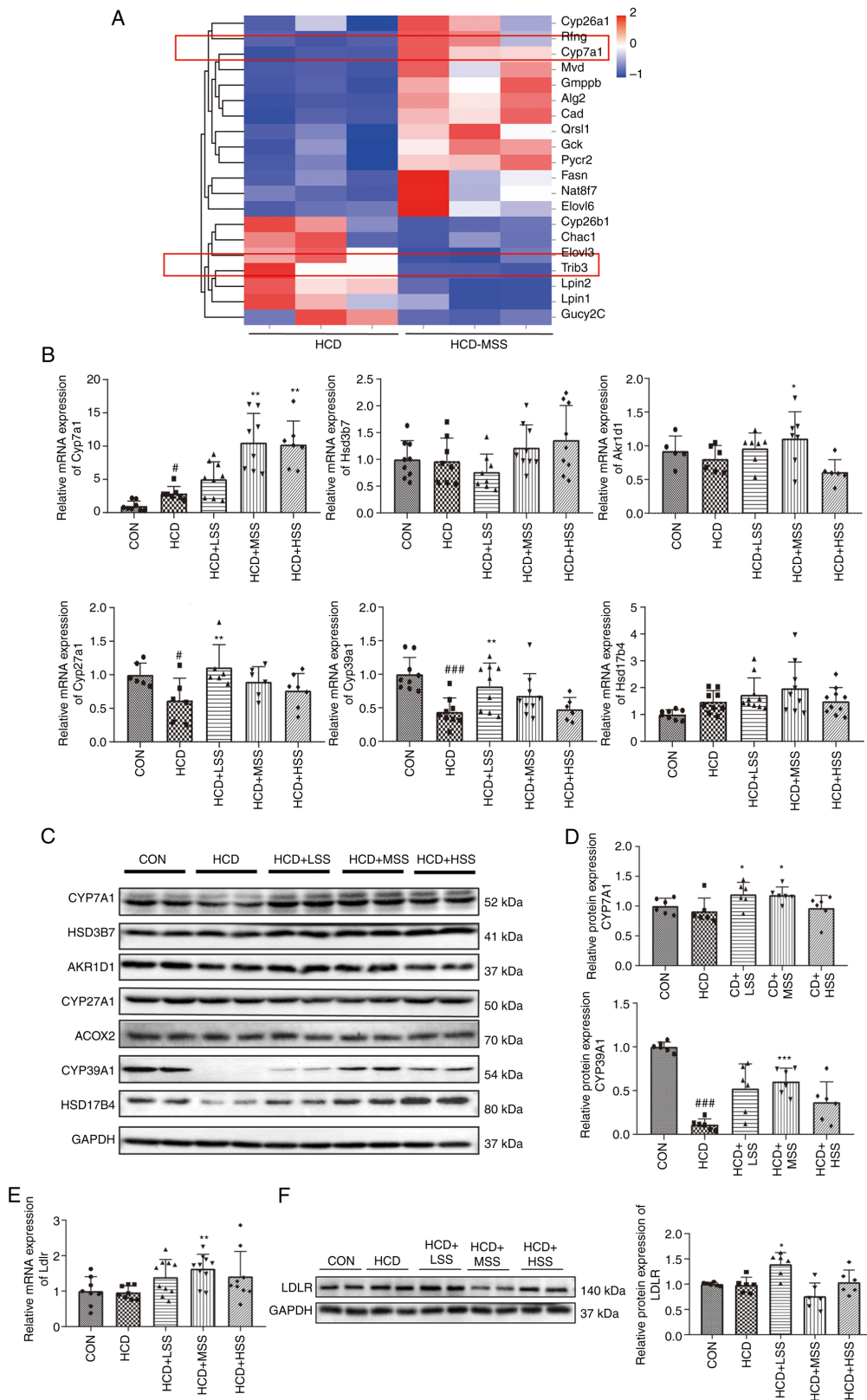


Figure 2. Effect of sodium sulphate on the hepatic expression of genes associated with bile acid synthesis in mice fed an HCD. (A) Heatmap of genes associated with glucose and lipid metabolism in the liver tissues of mice in the HCD and HCD + MSS groups. (B) Relative mRNA expression levels of *Cyp7a1*, *Hsd3b7*, *Akrl1d1*, *Cyp27a1*, *Cyp39a1* and *Hsd17b4* in the liver tissues of mice from five groups: CON, HCD, HCD + LSS, HCD + MSS and HCD + HSS. (C) Western blotting results for CYP7A1, HSD3B7, AKR1D1, CYP27A1, ACOX2, CYP39A1 and HSD17B4 in the liver tissues of mice from the five groups. (D) Semi-quantitative analysis of the CYP7A1 and CYP39A1 western blotting results. (E) Relative mRNA expression levels of *Ldlr* in the liver tissues of mice from the five groups. (F) Western blotting results for LDLR in the liver tissues of mice from the five groups. The right panel shows the semi-quantitative analysis. GAPDH was used as the internal control for all experiments. * $P < 0.05$, ** $P < 0.01$, *** $P < 0.001$ vs. the CON group; * $P < 0.05$, ** $P < 0.01$, *** $P < 0.001$ vs. the HCD group. HCD, high cholesterol diet; CON, control; LSS, low dose of sodium sulphate; MSS, middle dose of sodium sulphate; HSS, high dose of sodium sulphate; Cyp7/27/39a1, cytochrome P450 family 7/27/39 subfamily A member 1; HSD3B7, hydroxy- δ -5-steroid dehydrogenase, 3 β - and steroid δ -isomerase 7; AKR1D1, aldo-keto reductase family 1 member D1; HSD17B4, hydroxysteroid 17- β dehydrogenase 4; ACOX2, acyl-CoA oxidase 2; LDLR, low density lipoprotein receptor.

compared with the HCD group (Fig. 2C and D). The mRNA levels of *Akr1d1* in the HCD + MSS group and *Cyp27a1* in the HCD + LSS group were significantly upregulated compared with those in the HCD group (Fig. 2B), but no marked change in the AKR1D1 and CYP27A1 protein levels was observed among the five groups (Fig. 2C). The mRNA and protein expression levels of CYP39A1 were significantly reduced in the hepatic tissues from the HCD group compared with the CON group (Fig. 2B-D). In addition, the hepatic *Cyp39a1* mRNA expression levels were significantly upregulated in the HCD + LSS group compared with the HCD group (Fig. 2B), and the CYP39A1 protein expression level was significantly higher in the hepatic tissues from mice in the HCD + MSS group compared with the HCD group (Fig. 2C and D). No significant difference in the *Ldlr* mRNA level was detected between the hepatic tissues of the HCD and CON groups (Fig. 2E). However, the *Ldlr* transcriptional level was significantly higher in the hepatic tissues from mice in the HCD + MSS group compared with the HCD group (Fig. 2E). The *Ldlr* mRNA levels in the livers of mice from the HCD + LSS and HCD + HSS groups were also increased compared with the *Ldlr* mRNA level in the CON group, but this increase was not significant (Fig. 2E). The western blotting results demonstrated that the LDLR protein level in the hepatic tissues of mice from the HCD + LSS group was also significantly increased compared with that in the HCD group (Fig. 2F). These results suggest that sodium sulphate might alleviate hypercholesterolemia in mice fed an HCD via upregulation of the expression of genes that encode enzymes that catalyze bile acid production, including *Cyp7a1* and *Cyp39a1*, and upregulation of the expression of *Ldlr*, which takes up excessive LDL-C from the blood into the hepatocytes of mice.

The hepatic expression levels of genes associated with cholesterol synthesis were also assessed. The mRNA expression levels of 3-hydroxy-3-methylglutaryl-CoA synthase 1, *Hmgcr*, *Mvk*, *Mvd*, *Idi1*, *Fdps*, *Fdft1*, squalene epoxidase, *Osc*, 7-dehydrocholesterol reductase and *Cyp51a1* in hepatic tissues from the HCD group were significantly reduced 2 to >10-fold compared with those in the CON group (Fig. S4A), and the levels of most of these mRNAs were slightly increased after sodium sulphate administration, some significantly, namely *Mvd*, *Idi1*, *Fdps* and *Cyp51a1* (Fig. S4A). However, the *Fdft1* mRNA levels in the hepatic tissues of mice from the HCD + MSS and HCD + HSS groups were markedly lower compared with those in the HCD group (Fig. S4A). At the protein level, the expression of HMGCR, the rate-limiting enzyme of cholesterol biosynthesis (29,30), was not significantly different among the five groups. However, the MVK, MVD, IDI1, FDPS, FDFT1 and LSS levels were all notably downregulated in the hepatic tissues from the HCD group compared with the CON group, and were not affected by sodium sulphate administration (Fig. S4B).

Sodium sulphate improves insulin resistance in the livers of mice fed an HCD. The RNA-seq results demonstrated that the expression of *Trib3*, the mRNA that encodes TRB3, was significantly reduced in the livers of mice from the HCD + MSS group compared with the HCD group (Fig. 2A). Increased *Trib3* expression is known to cause insulin resistance in hepatocytes *in vivo* and *in vitro* (31-34). KEGG analysis of

the mRNAs in the livers of the mice that were differentially expressed between the HCD and the HCD + MSS groups indicated that 'Insulin signaling pathway' and 'Insulin resistance' were among the top 10 pathways that affected the HCD group following sodium sulphate administration (Fig. 3A). The results of RT-qPCR and western blotting analysis demonstrated that *Trib3* expression was significantly increased in the hepatic tissues of mice from the HCD group compared with the CON group, at the mRNA and protein levels (Fig. 3B). The *Trib3* mRNA levels were significantly reduced in the hepatic tissues of mice fed an HCD following the administration of sodium sulphate (Fig. 3B). In addition, the TRB3 protein levels were significantly lower in the hepatic tissues of mice from the HCD + LSS and HCD + MSS groups compared with the HCD group (Fig. 3B).

Furthermore, the activation and protein levels of components of the insulin signal pathways were evaluated by the western blotting. The p-IRS1 (Tyr608) protein levels in the hepatic tissues from the HCD + LSS, HCD + MSS and HCD + HSS groups were higher compared with those in the CON and HCD groups (Fig. 3C). The p-AKT levels in the hepatic tissues of mice from the HCD group were lower compared with those in the CON group, and the administration of sodium sulphate to HCD-fed mice increased these levels (Fig. 3C). The ratio of p-AKT/AKT was significantly lower in liver tissue from the HCD group compared with the CON group, and was significantly increased in the HCD + MSS and HCD + HSS groups compared with the HCD group (Fig. 3C). These results indicate that sodium sulphate attenuated the hepatic insulin resistance in mice fed an HCD by inhibiting the expression of *Trib3* in hepatocytes.

Sodium sulphate inhibits the FGF15/FGF4-Klb/JNK/c-Jun signaling pathway in the hepatocytes of mice fed an HCD. A number of studies have confirmed that the reduction of FGF15 expression in the ileum can induce the expression of *Cyp7a1* in hepatocytes to increase the conversion of cholesterol to bile acid (13,35,36). Therefore, the *Fgf15* mRNA expression levels in the ileum of mice from the five groups were assessed using RT-qPCR. The *Fgf15* transcriptional level in the HCD group was slightly lower than that in the CON group, but the reduction was not significant (Fig. 4A). The *Fgf15* mRNA levels were lower in the HCD + LSS, HCD + MSS and HCD + HSS groups compared with the HCD group, but these changes were also not significant (Fig. 4A). However, it is speculated that sodium sulphate may inhibit the expression of FGF15 in the ileum of mice fed an HCD. In the hepatic tissues, the mRNA expression level of *Fgfr4*, which encodes the receptor for FGF15 (15,37), was significantly reduced in the HCD group compared with the CON group, and was unaffected by the administration of sodium sulphate (Fig. 4B). No significant differences in the mRNA and protein expression levels of KLB, which is the co-receptor of FGFR4 (14), were detected in the hepatic tissues from mice in the CON and HCD groups (Fig. 4C and D). However, the *Klb* mRNA levels were significantly downregulated in the hepatic tissues from mice fed an HCD following the administration of sodium sulphate, and the KLB protein levels were also significantly lower in the hepatic tissues of mice from the HCD + MSS and HCD + HSS groups compared with the HCD group (Fig. 4C and D). These results

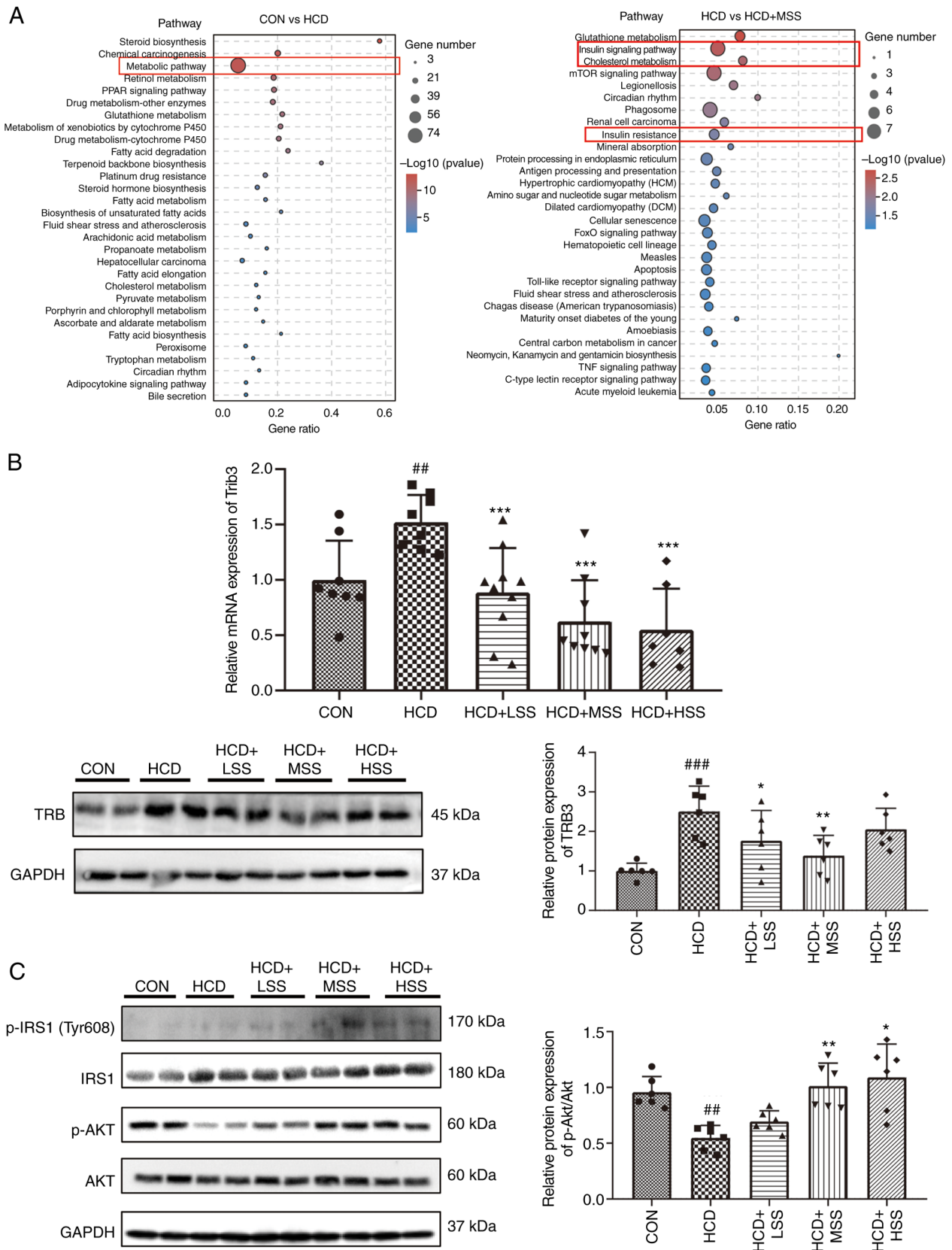


Figure 3. Effect of sodium sulphate on the insulin signaling pathway in the liver tissues of mice fed an HCD. (A) Kyoto Encyclopedia of Genes and Genomes analysis of the biological pathways of differently expressed mRNAs in the livers of mice from the CON vs. HCD and HCD vs. HCD + MSS groups. (B) RT-qPCR and western blotting results of the *Trib3* mRNA and TRB3 protein expression levels in the liver tissues of mice from the CON, HCD, HCD + LSS, HCD + MSS and HCD + HSS groups, respectively. (C) Western blotting results showing the protein expression levels of p-IRS1 (Tyr608), IRS1, p-AKT and AKT in the liver tissues of mice from the CON, HCD, HCD + LSS, HCD + MSS and HCD + HSS groups. The right panel shows the semi-quantitative analysis of the p-AKT/AKT ratio. GAPDH was used as the internal control for western blotting and RT-qPCR. ## $P < 0.01$, ### $P < 0.001$ vs. the CON group; * $P < 0.05$, ** $P < 0.01$, *** $P < 0.001$ vs. the HCD group. HCD, high cholesterol diet; CON, control; LSS, low dose of sodium sulphate; MSS, middle dose of sodium sulphate; HSS, high dose of sodium sulphate; RT-qPCR, reverse transcription-quantitative PCR; Trib3/TRB3, tribbles pseudokinase 3; p-, phosphorylated; IRS1, insulin receptor substrate 1.

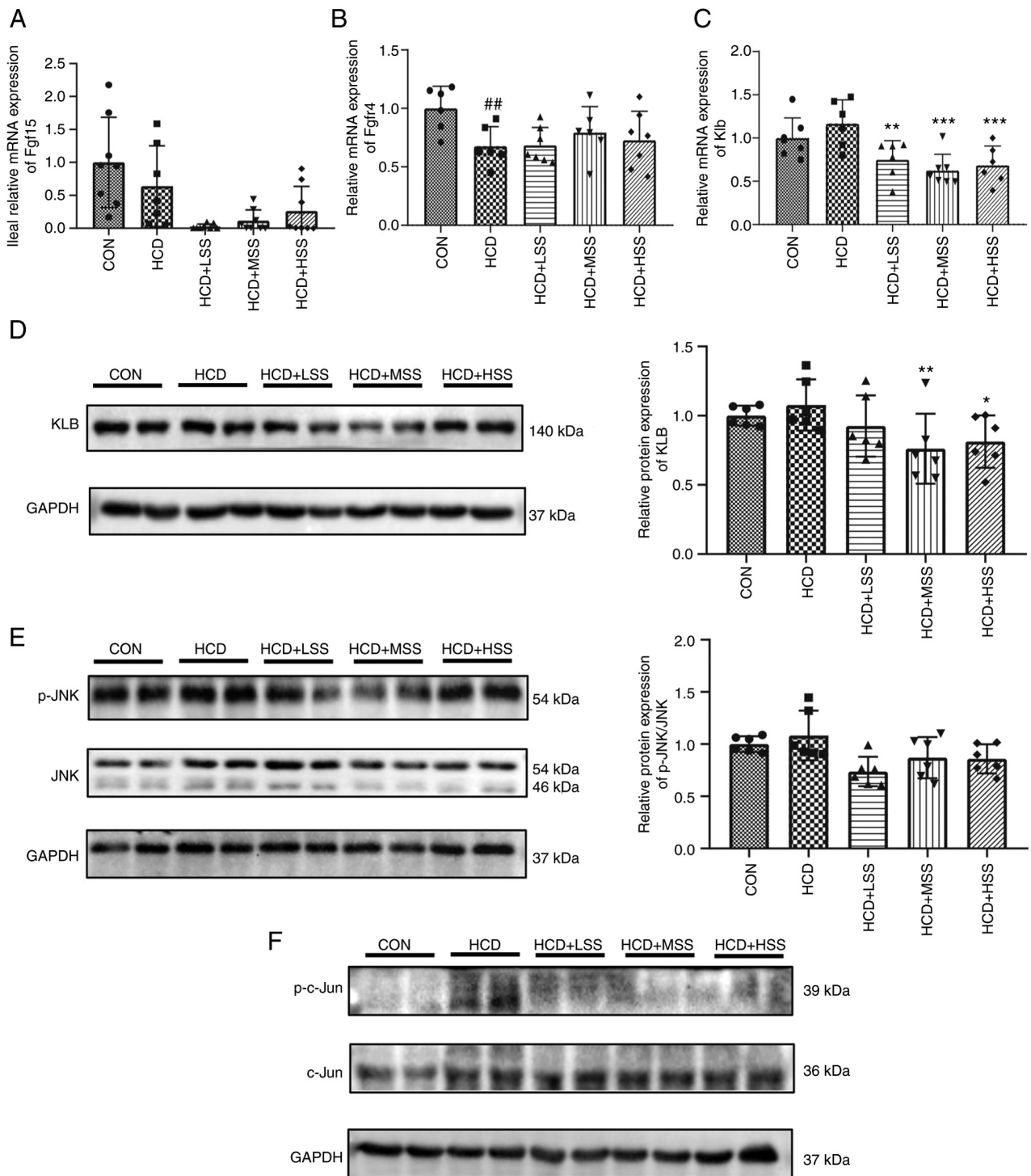


Figure 4. Effect of sodium sulphate on the FGF15/FGFR4-K1b/JNK signaling pathway in the livers of mice fed an HCD. Reverse transcription-quantitative PCR results of the relative mRNA expression levels of (A) *Fgf15* in the ileum and of (B) *Fgfr4* and (C) *Klb* in the liver tissues of mice from the five study groups: CON, HCD, HCD + LSS, HCD + MSS and HCD + HSS. (D) Western blotting results showing the protein expression level of KLB in the liver tissues of mice from the five groups. GAPDH was used as the internal control. The right panel shows the semi-quantitative analysis. (E) The p-JNK and JNK protein expression levels in the livers of mice from the five groups. The right panel shows the semi-quantitative analysis of the p-JNK/JNK ratio. (F) Western blotting results showing the p-c-Jun and c-Jun protein expression levels in the liver tissues of mice from the five groups. GAPDH was used as the internal control. ##P<0.01 vs. the CON group; *P<0.05, **P<0.01, ***P<0.001 vs. the HCD group. HCD, high cholesterol diet; CON, control; LSS, low dose of sodium sulphate; MSS, middle dose of sodium sulphate; HSS, high dose of sodium sulphate; FGF, fibroblast growth factor; FGFR, FGF receptor; KLB, Klotho β ; JNK, c-Jun N-terminal kinase; p-, phosphorylated.

demonstrate that the FGF15 signal in the hepatocytes of HCD fed mice treated with sodium sulphate might weaken due to the downregulation of FGF15 in the ileum and the reduction of KLB expression in the liver of these mice.

JNK is an important kinase that is activated by FGF15 signaling to inhibit the transcription of *Cyp7a1* in hepatocytes (38,39). Activated JNK suppresses the expression of *Cyp7a1* via the activation of c-Jun (40). Therefore, the

activation and expression levels of JNK and its target, c-Jun, were further assessed using western blotting. The p-JNK/JNK ratio was slightly higher in the hepatic tissues of mice from the HCD group compared with the CON group, but this increase was not significant, and the administration of sodium sulphate reduced this ratio, although this reduction was also not significant (Fig. 4E). The p-c-Jun level was notably increased in the liver tissue of the HCD group compared with the CON group, and was decreased following administration of sodium sulphate (Fig. 4F). These results indicate that sodium sulphate may upregulate *Cyp7a1* expression via inhibition of the FGF15/FGFR4-KLB/JNK/c-Jun signaling pathway to promote the conversion of cholesterol to bile acid.

Sodium sulphate changes the composition and function of the gut microbiota in mice fed an HCD. The gut microbiota has been demonstrated to have an important role in regulating the lipid metabolism of the host (41). Therefore, 16S rDNA sequencing was performed to analyze the composition and function of the gut microbiota of mice from the CON, HCD, HCD + LSS, HCD + MSS and HCD + HSS groups. The Shannon rarefaction curves of each group reached the saturation plateau (Fig. 5A), indicating that the sequence coverage of the fecal samples was sufficient to describe the composition of the gut microbiota of all groups. Principal coordinate analysis demonstrated that the five groups were significantly distinguished (Fig. 5B). At the phylum level, the proportional abundance of *Bacteroidetes* was significantly lower in the HCD group compared with the CON group, and was significantly reduced in the HCD + LSS and HCD + MSS groups compared with the HCD group (Fig. 5C and D). The proportional abundance of *Proteobacteria* was significantly higher in the HCD group compared with the CON group, and was significantly reduced in the HCD + LSS group compared with the HCD group (Fig. 5C and D). Furthermore, the proportional abundance of *Firmicutes* was significantly increased in the sodium sulphate treated groups compared with the HCD group (Fig. 5C and D).

The results of the LEFse analysis demonstrated that there were 147 bacterial taxa that differed in abundance between the CON and HCD groups, with 76 predominant in the CON group and 71 predominant in the HCD group (Fig. 6). There were 115 bacterial taxa that differed in abundance between the HCD and HCD + LSS groups, with 41 predominant in the HCD group and 74 predominant in the HCD + LSS group (Fig. 7). There were 91 bacterial taxa that differed in abundance between the HCD and HCD + MSS groups, with 31 predominant in the HCD group and 60 predominant in the HCD + MSS group (Fig. 8). There were 43 bacterial taxa that differed in abundance between the HCD and HCD + HSS groups, with 18 predominant in the HCD group and 25 predominant in the HCD+HSS group (Fig. 9). Compared with the HCD group, there were 13 predominant bacterial taxa in all three groups treated with sodium sulphate, including: Phylum, *Firmicutes*; order, *Clostridiales*; class, *Clostridia*; family, *Peptostreptococcaceae*; genus, *Ruminococcaceae_NK4A214_group*; family, *Family_XIII*; genus, *Eubacterium_nodatum_group*; species, *Ileibacterium_valens*; genus, *Ileibacterium*; genus, *Erysipelatoclostridium*; genus, *Eubacterium_brachy_group*; genus, *Sphingomonas*; and genus, *Faecalibaculum* (Figs. 7-9).

The top 20 altered pathways in the KEGG pathway analysis are shown in Fig. 10. These included 19 pathways that were significantly increased in all three sodium sulphate treated groups compared with the CON and HCD groups, including 'Biosynthesis of ansamycins', 'Valine, leucine and isoleucine biosynthesis', 'Biosynthesis of vancomycin group antibiotics', 'D-Glutamine and D-glutamate metabolism', 'Peptidoglycan biosynthesis', 'Alanine, aspartate and glutamate metabolism', 'One carbon pool by folate', 'Pantothenate and CoA biosynthesis', 'Streptomycin biosynthesis', 'Pentose phosphate pathway', 'Carbon fixation in photosynthetic organism', 'Aminoacyl-tRNA biosynthesis', 'D-Alanine metabolism', 'C5-Branched dibasic acid metabolism', 'Mismatch repair', 'Lysine biosynthesis', 'Ribosome', 'Fatty acid biosynthesis' and 'Cell cycle-Caulobacter'. Most of these pathways were also increased in the HCD group compared to the CON group, with the exception of 'D-Glutamine and D-glutamate metabolism', 'One carbon pool by folate', 'Carbon fixation in photosynthetic organism' and 'Mismatch repair'. The 'Other glycan degradation' pathway was significantly decreased in all three of the sodium sulphate treated groups compared with the CON and HCD groups, and also decreased in the HCD group compared with the CON group.

Discussion

In the present study, a novel role of sodium sulphate in the amelioration of hypercholesterolemia in mice fed an HCD was uncovered. Firstly, it was confirmed that the administration of sodium sulphate reduced the TC concentration and LDL-C/HDL-C ratio in the serum of mice fed an HCD. It was also found that sodium sulphate upregulated the expression of *Cyp7a1*, *Cyp39a1* and *Ldlr* in the hepatic tissues of mice fed an HCD to increase the conversion and uptake of cholesterol in hepatocytes. Subsequently, it was demonstrated that sodium sulphate attenuated the insulin resistance in the livers of mice fed an HCD via downregulation of the expression of *Trib3* to increase the activation of AKT in hepatocytes. Finally, it was shown that sodium sulphate regulated the expression of *Cyp7a1* via inhibition of the FGF15/FGFR4-KLB/JNK/c-Jun signaling pathway in the livers of mice fed an HCD. These results indicate the function and mechanisms of sodium sulphate in the reduction of hypercholesterolemia in mice fed an HCD.

Increased TC levels causes >2.6 million deaths every year worldwide, and one-third of coronary heart disease cases are caused by an elevated serum TC concentration (42). An increase in serum LDL-C concentration is also a risk factor of ASCVD (43). The serum LDL-C level in patients with homozygous familial hypercholesterolemia patients is highly elevated and accelerates premature ASCVD (44). In the present study, sodium sulphate significantly reduced the serum concentration of TC and the LDL-C/HDL-C ratio in mice that were administered an HCD. These results indicate that sodium sulphate may be used to control and treat atherosclerosis and ASCVD. Mirabilite has been used in traditional Chinese medicine for nearly 2,000 years (6). Mirabilite is one of the four herbs of the traditional Chinese formulation Da-Cheng-Qi-Tang that is used to treat atherosclerosis (45,46). However, it is unclear which herb of the Da-Cheng-Qi-Tang has an anti-atherosclerotic function. The results of the present

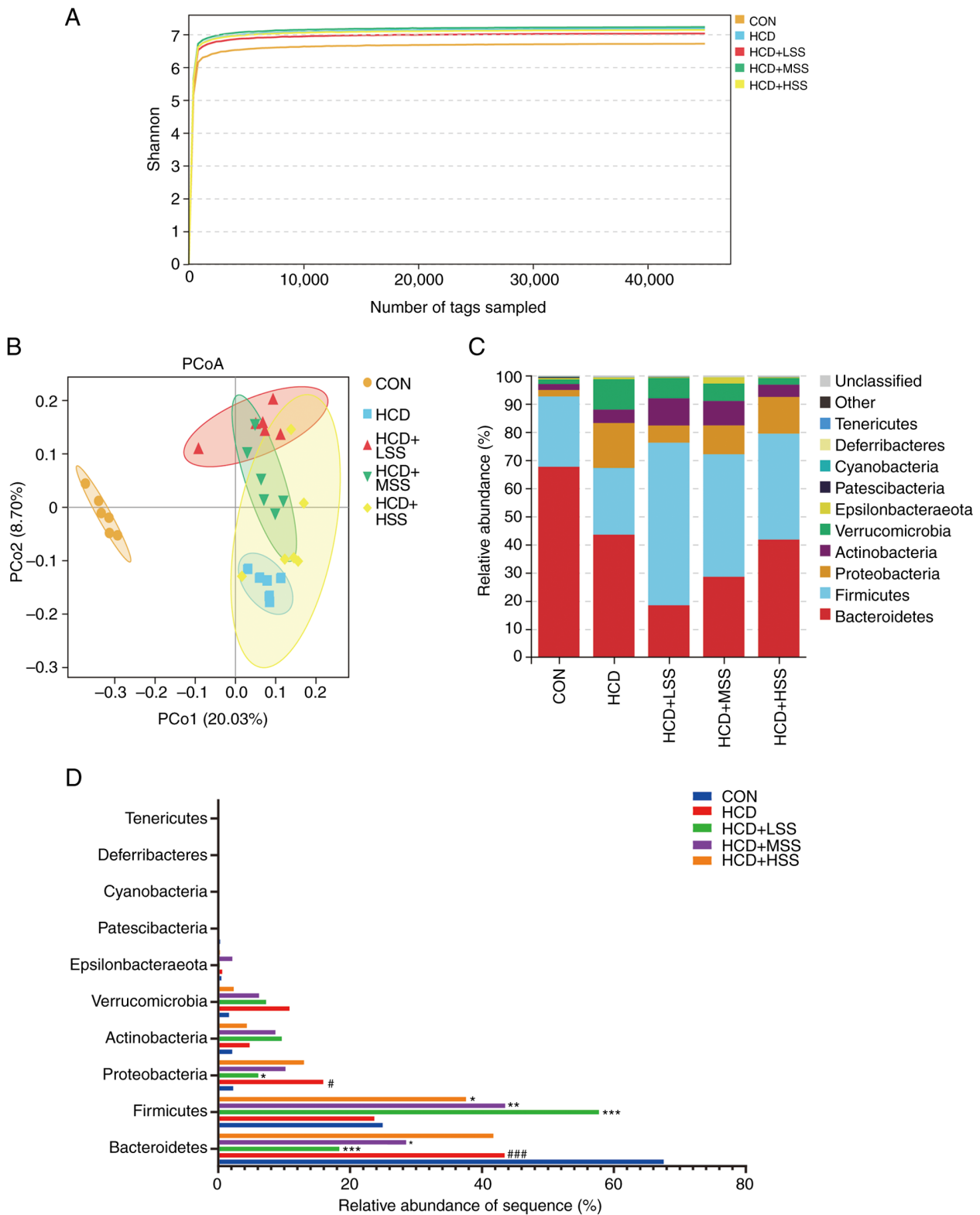


Figure 5. Sodium sulphate changed the relative abundance of the gut microbiota in mice fed an HCD. (A) Shannon rarefaction curves for the five study groups: CON, HCD, HCD + LSS, HCD + MSS and HCD + HSS. (B) The PCoA analysis of the gut microbiota from mice in the five groups. (C) Relative abundance of the gut microbiota at the phylum level from mice in the five groups. The different colors indicate different flora. (D) Bar chart of the proportional abundance of the gut microbiota at the phylum level in mice from the five groups. #P<0.05, ###P<0.001 vs. the CON group; *P<0.05, **P<0.01, ***P<0.001 vs. the HCD group. HCD, high cholesterol diet; CON, control; LSS, low dose of sodium sulphate; MSS, middle dose of sodium sulphate; HSS, high dose of sodium sulphate; PCoA, principal coordinate analysis.

study indicate that sodium sulphate, the effective ingredient of mirabilite, might be active against atherosclerosis since it attenuates hypercholesterolemia in mice.

CYP7A1 plays an important role in the maintenance of the homeostasis of cholesterol and bile acid *in vivo* (47). *Cyp7a1*^{-/-} mice exhibit a marked reduction in bile acid synthesis (48)

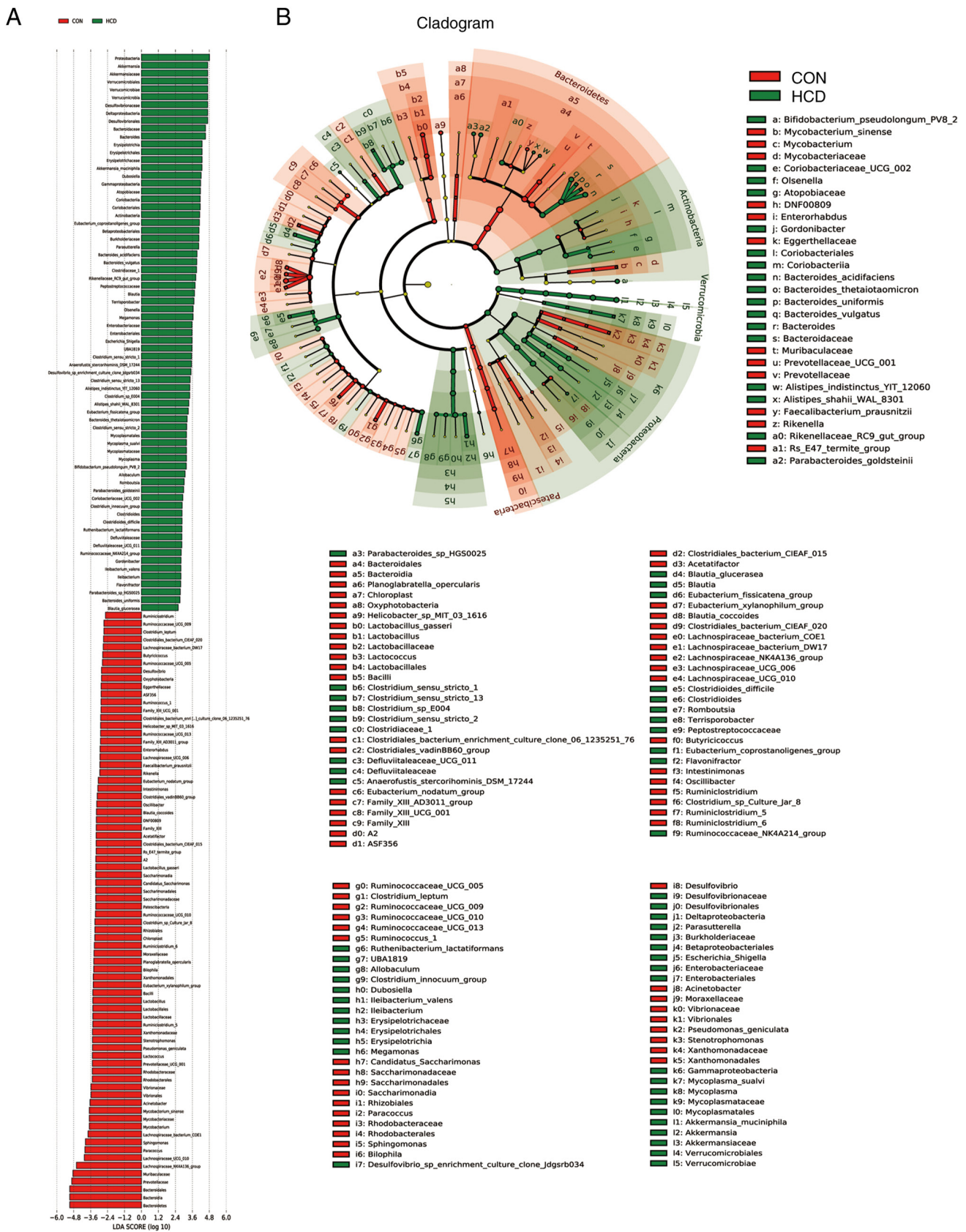


Figure 6. LDA effect size showing the predominant taxa for the CON and HCD groups. (A) LDA scores and (B) cladogram showing the predominant abundant taxa for the CON and HCD groups. Red represents bacteria specific for the CON group and green represents bacteria specific for the HCD group. CON, control; HCD, high cholesterol diet; LDA, linear discriminant analysis.

and exacerbated alcohol-induced hepatic inflammation and injury (49). A number of studies have demonstrated that the

upregulation of *Cyp7a1* in the liver reduces the serum cholesterol concentration in rat and mouse models. For example, it

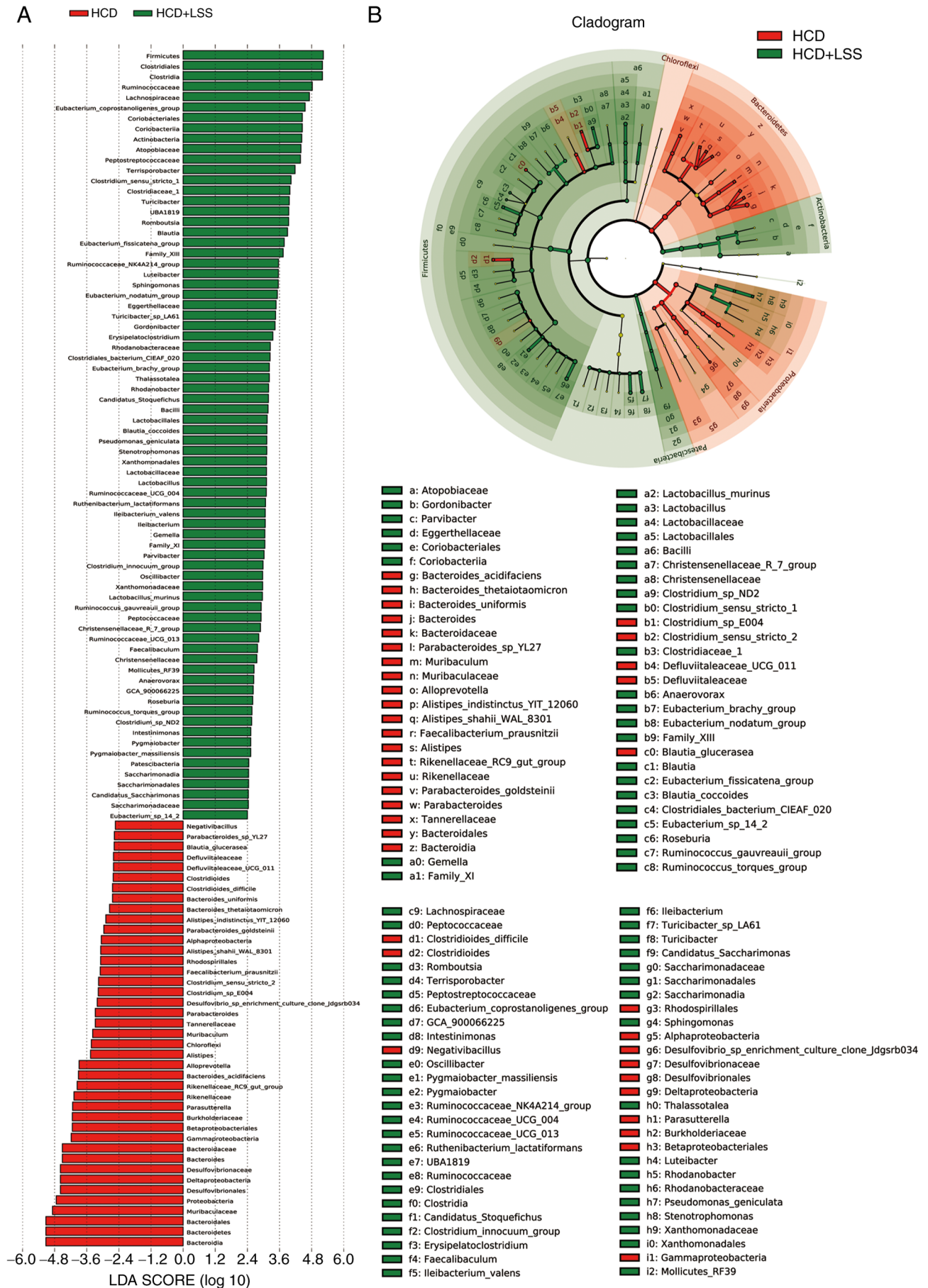


Figure 7. LDA effect size showing the predominant taxa for the HCD and HCD + LSS groups. (A) LDA scores and (B) cladogram showing the predominant abundant taxa for the HCD and HCD + LSS groups. Red represents bacteria specific for the HCD group and green represents bacteria specific for the HCD + LSS group. HCD, high cholesterol diet; LSS, low dose of sodium sulphate; LDA, linear discriminant analysis.

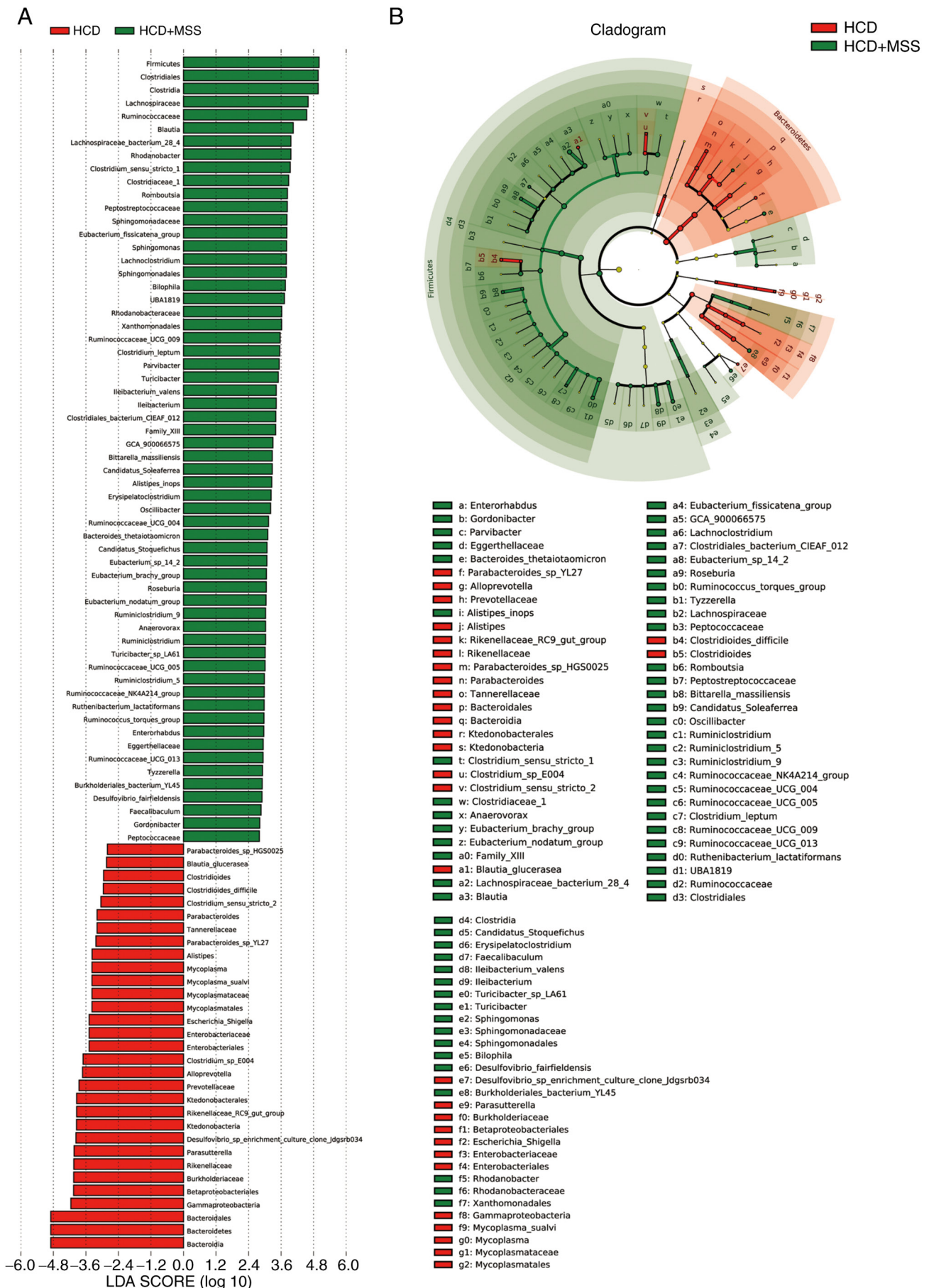


Figure 8. LDA effect size showing the predominant taxa for the HCD and HCD + MSS groups. (A) LDA scores and (B) cladogram showing the predominant abundant taxa for the HCD and HCD + MSS groups. Red represents bacteria specific for the HCD group and green represents bacteria specific for the HCD + MSS group. HCD, high cholesterol diet; MSS, middle dose of sodium sulphate; LDA, linear discriminant analysis.

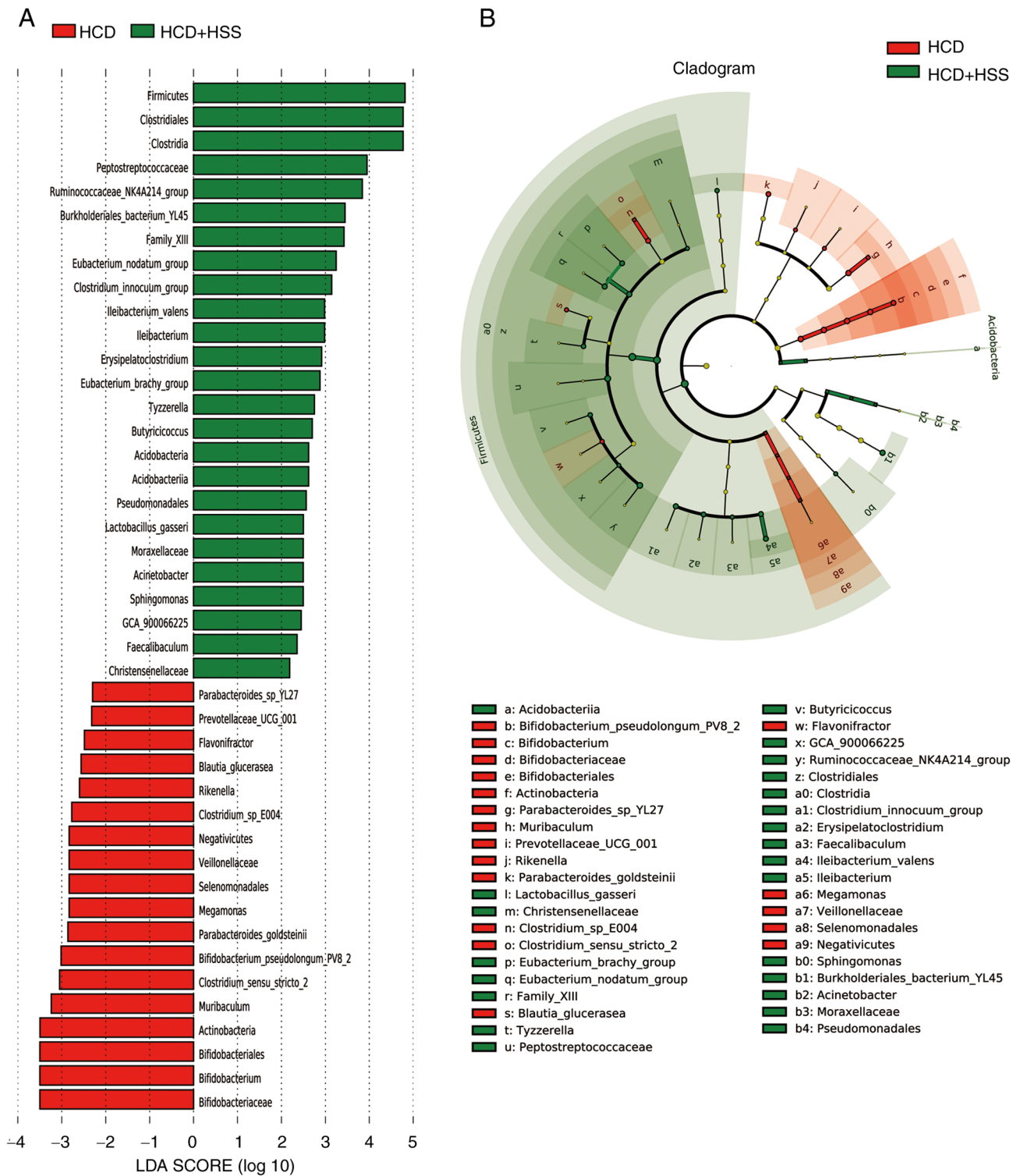


Figure 9. LDA effect size showing the predominant taxa for the HCD and HCD + HSS groups. (A) LDA scores and (B) cladogram showing the predominant abundant taxa for the HCD and HCD + HSS groups. Red represents bacteria specific for the HCD group and green represents bacteria specific for the HCD + HSS group. HCD, high cholesterol diet; HSS, high dose of sodium sulphate; LDA, linear discriminant analysis.

was reported that diosgenin attenuated hypercholesterolemia in rats fed a high-fat diet (HFD) via regulation of the scavenger receptor class B type 1/coxylesterase-1/CYP7A1/FXR pathway, and *Cyp7a1* was significantly upregulated by diosgenin in the livers of HFD-fed rats (50). In addition, it has been found that flavonoids from mulberry leaves and their active metabolite, quercetin reduce excessive cholesterol

accumulation in rats with orotic acid-induced NAFLD, and upregulate the expression of *Cyp7a1* in the hepatic tissue of these rats (51). Furthermore, in another study tomato seed oil reduced the concentration of TC, TG and LDL-C and the LDL-C/HDL-C ratio in the plasma of mice fed an HFD by increasing the expression of hepatic peroxisome proliferator-activated receptor α , acyl-CoA-dehydrogenase long chain,

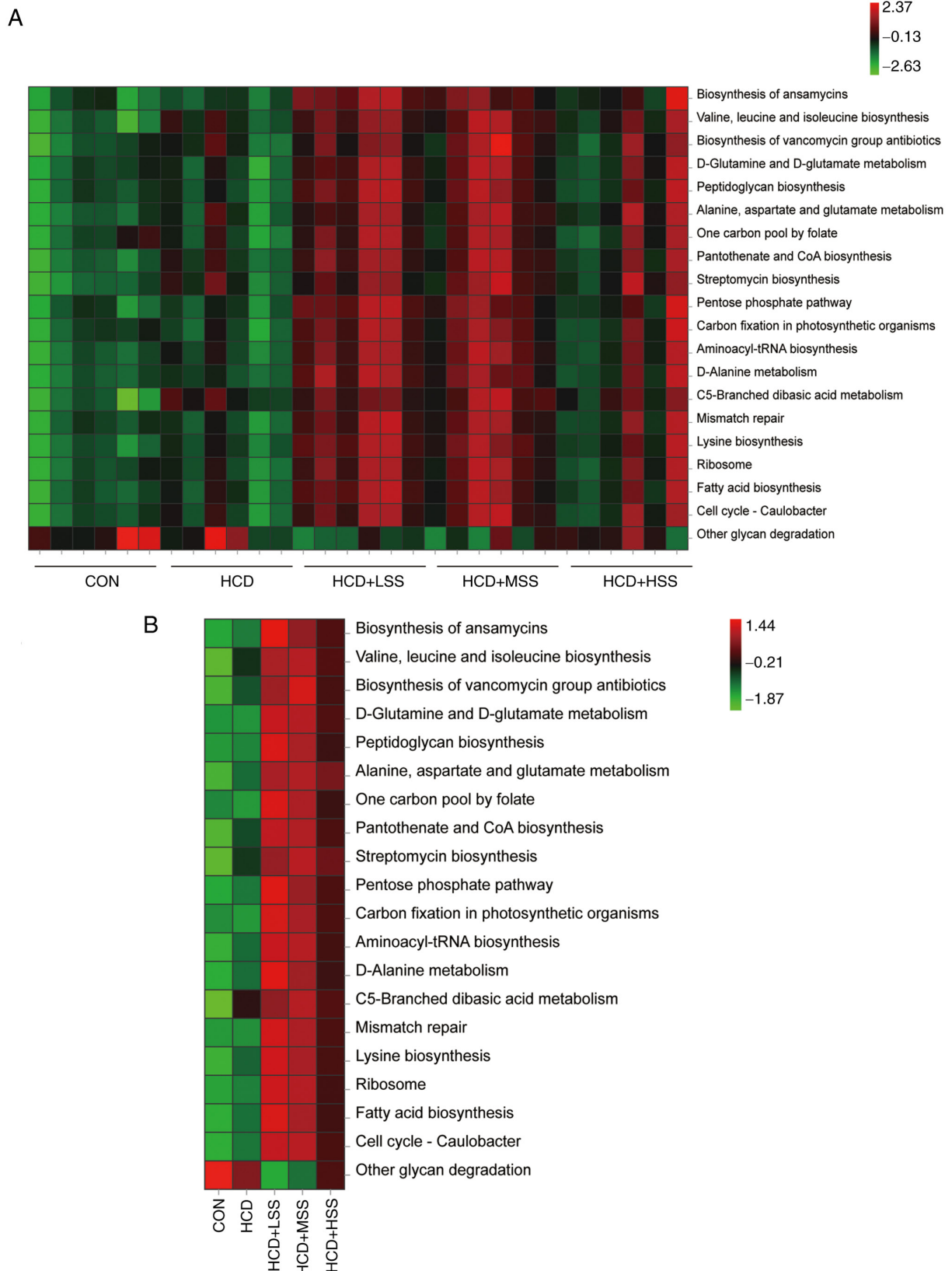


Figure 10. KEGG analysis of the gut microbiota from the CON, HCD, HCD + LSS, HCD + MSS and HCD + HSS groups. KEGG analysis showing the top 20 altered pathways in the gut microbiota of (A) each mouse in these groups and (B) of each group. KEGG, Kyoto Encyclopedia of Genes and Genomes; CON, control; HCD, high cholesterol diet; LSS, low dose of sodium sulphate; MSS, middle dose of sodium sulphate; HSS, high dose of sodium sulphate.

CYP7A1, liver X receptor α , ATP binding cassette subfamily A member 1 and scavenger receptor class B type 1 (52). *Cyp39a1* is one of the key genes in the synthesis of bile acid via the

mevalonate pathway (53). It has been shown that the activation of pregnane X receptor induces hypercholesterolemia in wild-type mice and accelerates atherosclerosis in *ApoE*^{-/-} mice,

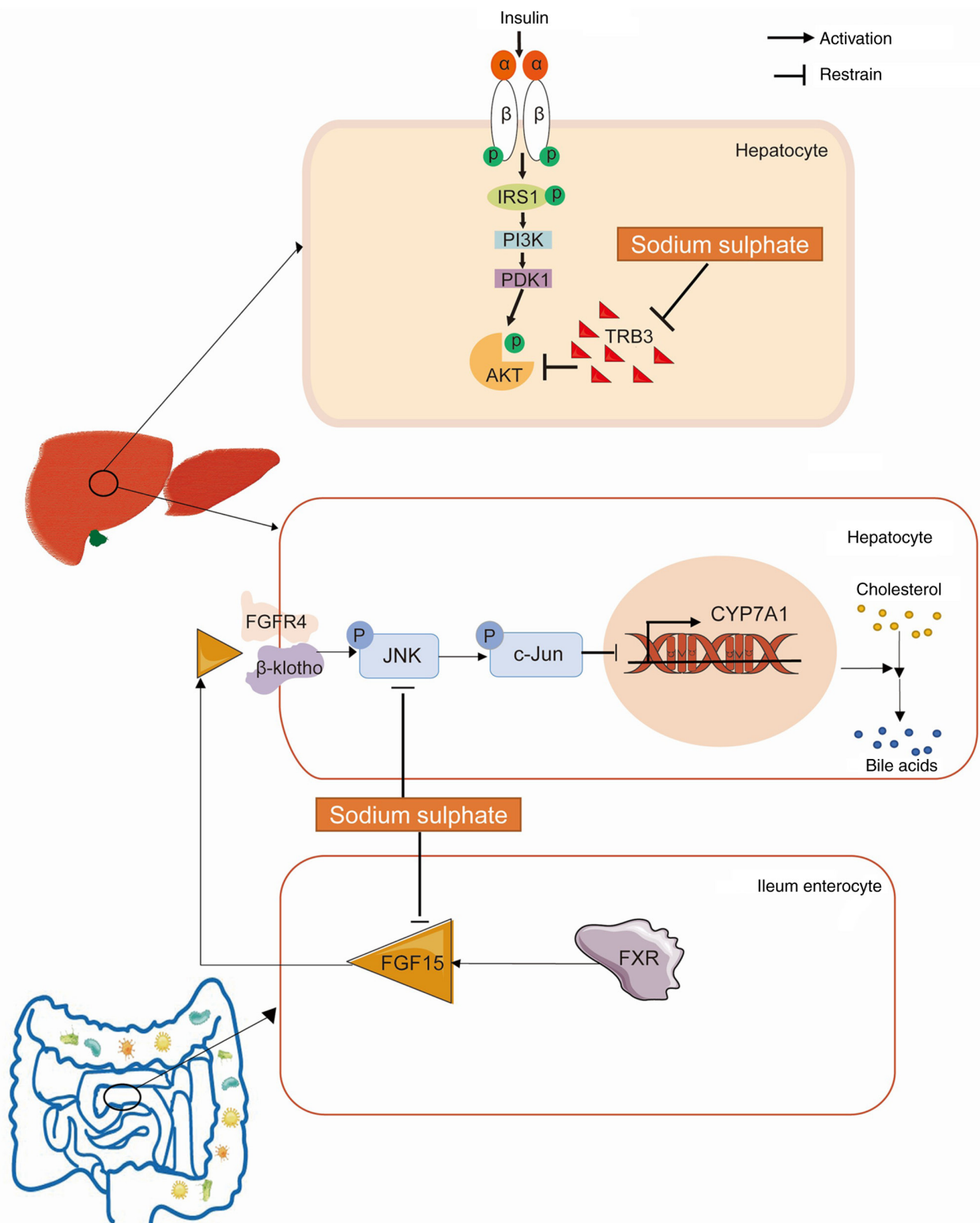


Figure 11. Sodium sulphate ameliorates hypercholesterolemia and hepatic insulin resistance in mice fed an HCD. Sodium sulphate inhibits the highly expressed TRB3 in the hepatocytes of mice fed an HCD, to attenuate the hepatic insulin resistance of these mice. In the enterocytes of the ileum, FGF15 expression is downregulated following the administration of sodium sulphate to mice fed an HCD. In addition, the hepatic expression of KLB, which is the co-receptor of FGFR4 for FGF15 binding, is significantly downregulated by sodium sulphate, and reduces the activation of JNK, which is downstream of the FGF15/FGFR4-KLB signaling pathway. The activation of c-Jun, which is the major target of p-JNK, is notably reduced, and the expression of *Cyp7a1*, which is inhibited by p-c-Jun, is significantly increased, which enhances the conversion of cholesterol to bile acids in these mice. HCD, high cholesterol diet; TRB3, tribbles homolog 3; FGF, fibroblast growth factor; FGFR, FGF receptor; KLB, Klotho β ; JNK, c-Jun N-terminal kinase; p-, phosphorylated; IRS1, insulin receptor substrate 1; PDK1, 3-phosphoinositide-dependent kinase 1; FXR, farnesoid X receptor.

while significantly repressing the *Cyp39a1* expression level in the livers of these mice (54). Hence, *Cyp39a1* is also essential

for the metabolic elimination of cholesterol *in vivo*. In the present study, the expression of *Cyp7a1* and *Cyp39a1* in the

hepatic tissues of mice fed an HCD was significantly upregulated by the administration of sodium sulphate, indicating that sodium sulphate enhances the conversion of cholesterol to bile acids in the mouse hepatocytes. The administration of sodium sulphate also increased hepatic *Ldlr* expression in the mice fed an HCD, and the upregulation of *Ldlr* or increase in LDLR activity results in the removal of excessive LDL-C from the circulation (55). The increase in the conversion of cholesterol to bile acids could also explain the changes in the composition and function of the gut microbiota in the present study since bile acids are important regulators of microbiota (56).

An increase in *Trib3* expression has been found to induce insulin resistance in the hepatocytes, myotubes and other types of cells (31,57-59). It has been reported that TRB3 protein expression is increased in the livers of elderly rats and is associated with insulin resistance (57). It has also been demonstrated that TRB3 is an endogenous inhibitor of AKT that inhibits the insulin signaling pathway (31). In addition, lipotoxicity has been shown to induce the upregulation of TRB3 and COP1, and thereby induce the degradation of sirtuin1, resulting in insulin resistance in hepatocytes *in vivo* and *in vitro* (58). Furthermore, in another study, TRPM2-activated Ca^{2+} signaling aggravated endothelial insulin resistance via the PERK/ATF4/TRB3 cascade in HFD-induced obese mice (59). In the present study, the administration of sodium sulphate significantly downregulated *Trib3* expression, which was significantly increased in the livers of mice fed an HCD, and alleviated the insulin resistance in the hepatic tissues caused by the HCD. These results indicate that sodium sulphate mitigates the insulin resistance induced by increased TRB3 expression in the liver and other tissues. The insulin resistance index will be determined in future studies to confirm the ability of sodium sulphate to ameliorate insulin resistance in mice fed an HCD.

Previous studies have confirmed that the FGF15/19 signaling pathway plays an important role in regulating *Cyp7a1* expression in hepatocytes. For example, in one study, blocking the ileum bile salt transporter SLC10A2 in HFD-fed Syrian golden hamsters significantly suppressed FGF15/19 expression in the ileum, and it was found that the reduced FGF15/19 signaling in hepatocytes upregulated the expression of *Cyp7a1* in the hepatic tissues of these animals via reduction of the phosphorylation of ERK1/2 and JNK in hepatocytes (38). In addition, it was reported that chronic overexpression of FGF21 in mice significantly upregulated the expression of *Cyp7a1*, as FGF21 antagonised the function of FGF15/19 as an inhibitor of *Cyp7a1* expression in hepatocytes (60). In the present study, the transcriptional levels of FGF15 were very low in the ileum of HCD-fed mice following the administration of sodium sulphate. We hypothesize that sodium sulphate inhibits the absorption of bile acid in the ileum of mice, then reduces the expression of FGF15 in these tissues, since the serum TBA concentrations in the serum of the sodium sulphate-treated mice were lower than those in the HCD group, albeit not significantly. The downregulation of FGF15 in the ileum of mice by sodium sulphate may be associated with the increase in *Cyp7a1* expression in hepatocytes.

FGF15/19 binds to FGFR4 and its co-receptor, KLB, on hepatic membranes to inhibit *Cyp7a1* expression in hepatocytes (61,62). In a previous study, FGFR4^{-/-} mice exhibited upregulated hepatic *Cyp7a1* expression and elevated bile-acid

excretion (63). In another study, it was reported that the expression of *Cyp7a1* and *Cyp8b1* was highly upregulated in the livers of *Klb* knockout mice, and the synthesis and excretion of bile acid were also notably increased in these mice (64). Therefore, the downregulation of *Klb* in the livers of mice could be another mechanism by which sodium sulphate increases the expression of *Cyp7a1* in hepatocytes and elevates the synthesis of bile acid in mice fed an HCD. It has been confirmed that FGF15/19 signaling downregulates the expression of *Cyp7a1* via the ERK1/2 and JNK pathways in hepatocytes (65). In the present study, the phosphorylation of JNK and its major target, c-Jun, was downregulated in the livers of mice fed an HCD after the administration of sodium sulphate for 3 weeks. Therefore, we hypothesize that sodium sulphate ameliorates the hypercholesterolemia in mice caused by HCD via inhibition of the FGF15/FGFR4-KLB/JNK/c-Jun signaling pathway in hepatocytes. The inhibition of this pathway might affect the gut microbiota due to the increase in the production of bile acids in the liver, although it is unclear whether sodium sulphate inhibits the FGF15/FGFR4-KLB/JNK/c-Jun pathway directly or via the regulation of the gut microbiota. In addition, JNK activation might promote the serine phosphorylation of IRS1 to reduce the p-AKT/AKT ratio in the insulin signaling pathway in hepatocytes (66). Hence, inhibition of the FGF15/FGFR4-KLB/JNK/c-Jun pathway might be a mechanism by which sodium sulphate increases the p-AKT/AKT ratio in the insulin signal pathway in hepatocytes.

In the present study, the *Firmicutes* phylum was significantly increased in mice treated with sodium sulphate. A previous study found that oatmeal reduced the levels of TC and LDL-C in patients with hypercholesterolemia, and the *Firmicutes* phylum was also significantly increased in the fecal microbiota of these patients (67). It has also been reported that the gut microbiota in ob/ob mice have upregulated KEGG pathways associated with the breakdown of indigestible dietary polysaccharides, such as butanoate metabolism, galactose metabolism and starch/sucrose metabolism, to increase the energy harvest for the host (68). In the present study, the KEGG analysis demonstrated that the pathways for 'Peptidoglycan biosynthesis' and 'Carbon fixation in photosynthetic organism' were increased, and the pathway for 'Other glycan degradation' was decreased in mice following treatment with sodium sulphate. We hypothesize that the changes in the composition and functions of the gut microbiota in mice treated with sodium sulphate might reduce the extraction of energy from food by the host. Furthermore, the reduced metabolic extraction might improve the reduced p-AKT/AKT ratio in the insulin signaling pathway in the hepatocytes of mice fed an HCD.

In conclusion, sodium sulphate mitigated the hypercholesterolemia and hepatic insulin resistance in mice fed an HCD (Fig. 11). Sodium sulphate also downregulated the highly expressed *Trib3* in the hepatocytes of HCD-fed mice to alleviate hepatic insulin resistance in these mice. In the enterocytes of the ileum from mice fed an HCD, the expression of FGF15 was downregulated by the administration of sodium sulphate. In addition, the hepatic expression of KLB, which is the co-receptor of FGFR4 in the binding of FGF15, was also significantly downregulated by sodium sulphate, and the activation of JNK, which is downstream of FGF15/FGFR4, was also reduced. Furthermore, the activation of c-Jun, which

is the major target of p-JNK, was also reduced, and the expression of *Cyp7a1*, which is inhibited by p-c-Jun, was significantly increased to enhance the conversion of cholesterol to bile acids in mice fed an HCD. In future, it would be worthwhile to explore the ability of sodium sulphate to alleviate the serum levels of TC and LDL-C in animal models of familial hypercholesterolemia.

Acknowledgements

Not applicable.

Funding

This study was supported by the National Natural Science Foundation of China (grant nos. 81830113, 81803912 and 82171855); National key R & D plan 'Research on modernization of traditional Chinese medicine' (grant no. 2018YFC1704200); Major basic and applied basic research projects of Guangdong Province of China (grant no. 2019B030302005); the Guangdong Basic and Applied Basic Research Foundation (grant no. 2021A1515012383); the Opening Foundation of the Key Laboratory of Regenerative Biology, Guangzhou Institutes of Biomedicine and Health, Chinese Academy of Sciences (grant no. KLRB201807); the Science and Technology Planning Project of Guangzhou City (grant no. 201803010069); and the Science and Technology Project of Yue-Xiu District of Guangzhou (grant no. 2018-WS-011).

Availability of data and materials

The RNA-seq data is available from <https://www.ncbi.nlm.nih.gov/sra/PRJNA774883>. The other datasets generated or analysed during the current study are available from the corresponding author on reasonable request.

Authors' contributions

ZL, YY and JG designed the project and conceived the manuscript. YY, CY and SY analysed and interpreted the results of mRNA sequencing and the 16S rDNA sequences. YY and ZL wrote the draft of the manuscript and revised it critically. SY, HR, YY and CY established the mouse model and administered sodium sulphate. YY, SY, ZL, HR, CY, HW, TZ, FY, YN, LC, QH and QS performed the morphological, biochemical and molecular experiments, including serum and liver biochemical profiles, western blotting, RT-qPCR and H&E staining. SY, HR and CY created the figures and table. ZL and YY confirm the authenticity of all the raw data. All authors have read and approved the final version of the manuscript.

Ethics approval and consent to participate

The mouse experiments were approved by The Guangdong Pharmaceutical University Experimental Animal Ethics Committee (approval no. gdpulacspf2017030-1; Guangzhou, China).

Patient consent for publication

Not applicable.

Competing interests

The authors declare that they have no competing interests.

References

- Ruotsalainen AK, Mäkinen P and Ylä-Herttuala S: Novel RNAi-based therapies for atherosclerosis. *Curr Atheroscler Rep* 23: 45, 2021.
- World Health Organization (WHO): Cardiovascular diseases (CVDs). WHO, Geneva, 2021. <https://www.who.int/news-room/fact-sheets/detail/cardiovascular-diseases-cvds>. Accessed June 11, 2021.
- Zhang M, Deng Q, Wang L, Huang Z, Zhou M, Li Y, Zhao Z, Zhang Y and Wang L: Prevalence of dyslipidemia and achievement of low-density lipoprotein cholesterol targets in Chinese adults: A nationally representative survey of 163,641 adults. *Int J Cardiol* 260: 196-203, 2018.
- Meng XD, Yao HH, Wang LM, Yu M, Shi S, Yuan ZX and Liu J: Knockdown of GAS5 inhibits atherosclerosis progression via reducing EZH2-mediated ABCA1 transcription in ApoE(-/-) mice. *Mol Ther Nucl Acids* 19: 84-96, 2020.
- Tseng SH, Lee HH, Chen LG, Wu CH and Wang CC: Effects of three purgative decoctions on inflammatory mediators. *J Ethnopharmacol* 105: 118-124, 2006.
- Zhong XG, Zheng FJ, Li YH, Xu H, Wang Q, Liu YC, Liu M, Wu RH, Gao YS, Zhang SJ, *et al*: Specific link between lung and large intestine: A new perspective on neuropeptide secretion in lung with herbal laxative stimulation. *Evid Based Complement Alternat Med* 2013: 547837, 2013.
- Sun H, Zhang AH, Zhang HL, Zhou XH, Wang XQ, Liu L and Wang XJ: Ultra-performance liquid chromatography/mass spectrometry technology and high-throughput metabolomics for deciphering the preventive mechanism of mirabilite on colorectal cancer via the modulation of complex metabolic networks. *RSC Adv* 9: 35356-35363, 2019.
- Mottacki N, Simrén M and Bajor A: Review article: Bile acid diarrhoea-pathogenesis, diagnosis and management. *Aliment Pharmacol Ther* 43: 884-898, 2016.
- Jahnel J, Fickert P, Hauer AC, Högenauer C, Avian A and Trauner M: Inflammatory bowel disease alters intestinal bile acid transporter expression. *Drug Metab Dispos* 42: 1423-1431, 2014.
- Camilleri M and Vijayvargiya P: The role of bile acids in chronic diarrhea. *Am J Gastroenterol* 115: 1596-1603, 2020.
- Shin A, Camilleri M, Vijayvargiya P, Busciglio I, Burton D, Ryks M, Rhoten D, Lueke A, Saenger A, Girtman A and Zinsmeister AR: Bowel functions, fecal unconjugated primary and secondary bile acids, and colonic transit in patients with irritable bowel syndrome. *Clin Gastroenterol Hepatol* 11: 1270-1275.e1271, 2013.
- Kim YC, Seok S, Zhang Y, Ma J, Kong B, Guo G, Kemper B and Kemper JK: Intestinal FGF15/19 physiologically repress hepatic lipogenesis in the late fed-state by activating SHP and DNMT3A. *Nat Commun* 11: 5969, 2020.
- Fiorucci S, Distrutti E, Carino A, Zampella A and Biagioli M: Bile acids and their receptors in metabolic disorders. *Prog Lipid Res* 82: 101094, 2021.
- Wu X, Ge H, Lemon B, Weiszmann J, Gupta J, Hawkins N, Li X, Tang J, Lindberg R and Li Y: Selective activation of FGFR4 by an FGF19 variant does not improve glucose metabolism in ob/ob mice. *Proc Natl Acad Sci USA* 106: 14379-14384, 2009.
- Williams CM, Calderon JH, Hock E, Jimenez Y, Barringer K, Carbonaro M, Molina-Portela MDP, Thurston G, Li Z and Daly C: Monomeric/dimeric forms of Fgf15/FGF19 show differential activity in hepatocyte proliferation and metabolic function. *FASEB J* 35: e21286, 2021.
- de Vos WM, Tilg H, Van Hul M and Cani PD: Gut microbiome and health: Mechanistic insights. *Gut* 71: 1020-1032, 2022.
- Kriaa A, Bourgin M, Potiron A, Mkaouer H, Jablaoui A, Gérard P, Maguin E and Rhimi M: Microbial impact on cholesterol and bile acid metabolism: Current status and future prospects. *J Lipid Res* 60: 323-332, 2019.
- Le Roy T, Lécuyer E, Chassaing B, Rhimi M, Lhomme M, Boudebouze S, Ichou F, Barceló JH, Huby T, Guerin M, *et al*: The intestinal microbiota regulates host cholesterol homeostasis. *BMC Biol* 17: 94, 2019.
- Vourakis M, Mayer G and Rousseau G: The role of gut microbiota on cholesterol metabolism in atherosclerosis. *Int J Mol Sci* 22: 8074, 2021.

20. Tong LT, Xiao T, Wang L, Lu C, Liu L, Zhou X, Wang A, Qin W and Wang F: Plant protein reduces serum cholesterol levels in hypercholesterolemia hamsters by modulating the compositions of gut microbiota and metabolites. *iScience* 24: 103435, 2021.
21. Chen S, Zhou Y, Chen Y and Gu J: fastp: An ultra-fast all-in-one FASTQ preprocessor. *Bioinformatics* 34: i884-i890, 2018.
22. Love MI, Huber W and Anders S: Moderated estimation of fold change and dispersion for RNA-seq data with DESeq2. *Genome Biol* 15: 550, 2014.
23. Kanehisa M, Araki M, Goto S, Hattori M, Hirakawa M, Itoh M, Katayama T, Kawashima S, Okuda S, Tokimatsu T and Yamanishi Y: KEGG for linking genomes to life and the environment. *Nucl Acids Res* 36: D480-D484, 2007.
24. Zhuri D, Gurkan H, Eker D, Karal Y, Yalcintepe S, Atli E, Demir S and Atli EI: Investigation on the effects of modifying genes on the spinal muscular atrophy phenotype. *Global Med Gene* 9: 226-236, 2022.
25. Lei Z, Wu H, Yang Y, Hu Q, Lei Y, Liu W, Nie Y, Yang L, Zhang X, Yang C, *et al*: Ovariectomy impaired hepatic glucose and lipid homeostasis and altered the gut microbiota in mice with different diets. *Front Endocrinol (Lausanne)* 12: 708838, 2021.
26. Lennernäs H and Fager G: Pharmacodynamics and pharmacokinetics of the HMG-CoA reductase inhibitors. *Clin Pharmacokinet* 32: 403-425, 1997.
27. Liu A, Jin H, Dirsch O, Deng M, Huang H, Bröcker-Preuss M and Dahmen U: Release of danger signals during ischemic storage of the liver: A potential marker of organ damage? *Mediators Inflamm* 2010: 436145, 2010.
28. Tan D, Ling L, Qin L, Lu Y, Wu D and He Y: Rosiglitazone induces hepatocyte injury by increasing DCA accumulation through OATP1A4 inhibiting in mice. *Arab J Chem* 16: 105142, 2023.
29. Khan AA, Sundar P, Natarajan B, Gupta V, Arige V, Reddy SS, Barthwal MK and Mahapatra NR: An evolutionarily-conserved promoter allele governs HMG-CoA reductase expression in spontaneously hypertensive rat. *J Mol Cell Cardiol* 158: 140-152, 2021.
30. Zhong S, Li L, Liang N, Zhang L, Xu X, Chen S and Yin H: Acetaldehyde Dehydrogenase 2 regulates HMG-CoA reductase stability and cholesterol synthesis in the liver. *Red Biol* 41: 101919, 2021.
31. Cheng KK, Iglesias MA, Lam KS, Wang Y, Sweeney G, Zhu W, Vanhoutte PM, Kraegen EW and Xu A: APPL1 potentiates insulin-mediated inhibition of hepatic glucose production and alleviates diabetes via Akt activation in mice. *Cell Metab* 9: 417-427, 2009.
32. Du K, Herzig S, Kulkarni RN and Montminy M: TRB3: A tribbles homolog that inhibits Akt/PKB activation by insulin in liver. *Science* 300: 1574-1577, 2003.
33. Koo SH, Satoh H, Herzig S, Lee CH, Hedrick S, Kulkarni R, Evans RM, Olefsky J and Montminy M: PGC-1 promotes insulin resistance in liver through PPAR-alpha-dependent induction of TRB-3. *Nat Med* 10: 530-534, 2004.
34. Lei Z, Yang L, Yang Y, Niu Z, Zhang X, Song Q, Lei Y, Wu H and Guo J: Activation of Wnt/ β -catenin pathway causes insulin resistance and increases lipogenesis in HepG2 cells via regulation of endoplasmic reticulum stress. *Biochem Biophys Res Commun* 526: 764-771, 2020.
35. Zhang Z, Du Z, Liu Q, Wu T, Tang Q, Zhang J, Huang C, Huang Y, Li R, Li Y, *et al*: Glucagon-like peptide 1 analogue prevents cholesterol gallstone formation by modulating intestinal farnesoid X receptor activity. *Metabolism* 118: 154728, 2021.
36. Wang F, Zhao C, Yang M, Zhang L, Wei R, Meng K, Bao Y, Zhang L and Zheng J: Four citrus flavanones exert atherosclerosis alleviation effects in apoE(-/-) mice via different metabolic and signaling pathways. *J Agric Food Chem* 69: 5226-5237, 2021.
37. Gulfo J, Rotondo F, de León CG, Cornide-Petronio ME, Fuster C, Gracia-Sancho J, Jiménez-Castro MB and Peralta C: FGF15 improves outcomes after brain dead donor liver transplantation with steatotic and non-steatotic grafts in rats. *J Hepatol* 73: 1131-1143, 2020.
38. Ge MX, Niu WX, Ren JF, Cai SY, Yu DK, Liu HT, Zhang N, Zhang YX, Wang YC, Shao RG, *et al*: A novel ASBT inhibitor, IMB17-15, repressed nonalcoholic fatty liver disease development in high-fat diet-fed Syrian golden hamsters. *Acta Pharm Sin* 40: 895-907, 2019.
39. Jung D, York JP, Wang L, Yang C, Zhang A, Francis HL, Webb P, McKeehan WL, Alpini G, Lesage GD, *et al*: FXR-induced secretion of FGF15/19 inhibits CYP27 expression in cholangiocytes through p38 kinase pathway. *Pflugers Arch* 466: 1011-1019, 2014.
40. Gupta S, Stravitz RT, Dent P and Hylemon PB: Down-regulation of cholesterol 7 α -hydroxylase (CYP7A1) gene expression by bile acids in primary rat hepatocytes is mediated by the c-Jun N-terminal kinase pathway. *J Biol Chem* 276: 15816-15822, 2001.
41. Schoeler M and Caesar R: Dietary lipids, gut microbiota and lipid metabolism. *Rev Endocr Metab Disord* 20: 461-472, 2019.
42. Peters SA, Singhathe Y, Mackay D, Huxley RR and Woodward M: Total cholesterol as a risk factor for coronary heart disease and stroke in women compared with men: A systematic review and meta-analysis. *Atherosclerosis* 248: 123-131, 2016.
43. Cao J, Remaley AT, Guan W, Devaraj S and Tsai MY: Performance of novel low-density lipoprotein-cholesterol calculation methods in predicting clinical and subclinical atherosclerotic cardiovascular disease risk: The multi-ethnic study of atherosclerosis. *Atherosclerosis* 327: 1-4, 2021.
44. Wu Y, Jiang L, Zhang H, Cheng S, Wen W, Xu L, Zhang F, Yang Y, Wang L and Chen J: Integrated analysis of microRNA and mRNA expression profiles in homozygous familial hypercholesterolemia patients and validation of atherosclerosis associated critical regulatory network. *Genomics* 113: 2572-2582, 2021.
45. Ha KT, Kim JK, Lee YC and Kim CH: Inhibitory effect of Daesungki-Tang on the invasiveness potential of hepatocellular carcinoma through inhibition of matrix metalloproteinase-2 and -9 activities. *Toxic App Pharmacol* 200: 1-6, 2004.
46. Chung HJ, Kim DW, Maruyama I and Tani T: Effects of traditional Chinese formulations on rat carotid artery injured by balloon endothelial denudation. *Am J Chin Med* 31: 201-212, 2003.
47. Chiang JY: Bile acids: Regulation of synthesis. *J Lipid Res* 50: 1955-1966, 2009.
48. Schwarz M, Russell DW, Dietschy JM and Turley SD: Marked reduction in bile acid synthesis in cholesterol 7 α -hydroxylase-deficient mice does not lead to diminished tissue cholesterol turnover or to hypercholesterolemia. *J Lipid Res* 39: 1833-1843, 1998.
49. Donepudi AC, Ferrell JM, Boehme S, Choi HS and Chiang JYL: Deficiency of cholesterol 7 α -hydroxylase in bile acid synthesis exacerbates alcohol-induced liver injury in mice. *Hepatol Commun* 2: 99-112, 2018.
50. Yu L, Lu H, Yang X, Li R, Shi J, Yu Y, Ma C, Sun F, Zhang S and Zhang F: Diosgenin alleviates hypercholesterolemia via SRB1/CES-1/CYP7A1/FXR pathway in high-fat diet-fed rats. *Toxicol Appl Pharmacol* 412: 115388, 2021.
51. Hu Y, Xu J, Chen Q, Liu M, Wang S, Yu H, Zhang Y and Wang T: Regulation effects of total flavonoids in *Morus alba* L. on hepatic cholesterol disorders in orotic acid induced NAFLD rats. *BMC Complement Med Ther* 20: 257, 2020.
52. He WS, Li L, Rui J, Li J, Sun Y, Cui D and Xu B: Tomato seed oil attenuates hyperlipidemia and modulates gut microbiota in C57BL/6J mice. *Food Funct* 11: 4275-4290, 2020.
53. Zhang Y, Liu Y, Duan J, Wang H, Zhang Y, Qiao K and Wang J: Cholesterol depletion sensitizes gallbladder cancer to cisplatin by impairing DNA damage response. *Cell Cycle* 18: 3337-3350, 2019.
54. Zhou C, King N, Chen KY and Breslow JL: Activation of PXR induces hypercholesterolemia in wild-type and accelerates atherosclerosis in apoE deficient mice. *J Lipid Res* 50: 2004-2013, 2009.
55. Tiwari V and Khokhar M: Mechanism of action of anti-hypercholesterolemia drugs and their resistance. *Eur J Pharmacol* 741: 156-170, 2014.
56. Fuchs CD, Paumgartner G, Mlitz V, Kunczer V, Halilbasic E, Leditzig N, Wahlström A, Ståhlman M, Thüringer A, Kashofer K, *et al*: Colesevelam attenuates cholestatic liver and bile duct injury in *Mdr2(-/-)* mice by modulating composition, signaling and excretion of faecal bile acids. *Gut* 67: 1683-1691, 2018.
57. Gaspar RC, Muñoz VR, Nakandakari S, Vieira RFL, da Conceição LR, de Oliveira F, Crisol BM, da Silva ASR, Cintra DE, de Moura LP, *et al*: Aging is associated with increased TRB3, ER stress, and hepatic glucose production in the liver of rats. *Exp Gerontol* 139: 111021, 2020.
58. Ren X, Chen N, Chen Y, Liu W and Hu Y: TRB3 stimulates SIRT1 degradation and induces insulin resistance by lipotoxicity via COPI1. *Exp Cell Res* 382: 111428, 2019.
59. Sun L, Liu YL, Ye F, Xie JW, Zeng JW, Qin L, Xue J, Wang YT, Guo KM, Ma MM, *et al*: Free fatty acid-induced H(2)O(2) activates TRPM2 to aggravate endothelial insulin resistance via Ca(2+)-dependent PERK/ATF4/TRB3 cascade in obese mice. *Free Radic Biol Med* 143: 288-299, 2019.
60. Zhang J, Gupte J, Gong Y, Weiszmann J, Zhang Y, Lee KJ, Richards WG and Li Y: Chronic over-expression of fibroblast growth factor 21 increases bile acid biosynthesis by opposing FGF15/19 ACTION. *EBioMedicine* 15: 173-183, 2017.

61. Fu T, Kim YC, Byun S, Kim DH, Seok S, Suino-Powell K, Xu HE, Kemper B and Kemper JK: FXR primes the liver for intestinal FGF15 signaling by transient induction of β -Klotho. *Mol Endocrinol* 30: 92-103, 2016.
62. Kliewer SA and Mangelsdorf DJ: Bile acids as hormones: The FXR-FGF15/19 Pathway. *Dig Dis* 33: 327-331, 2015.
63. Yu C, Wang F, Kan M, Jin C, Jones RB, Weinstein M, Deng CX and McKeehan WL: Elevated cholesterol metabolism and bile acid synthesis in mice lacking membrane tyrosine kinase receptor FGFR4. *J Biol Chem* 275: 15482-15489, 2000.
64. Ito S, Fujimori T, Furuya A, Satoh J, Nabeshima Y and Nabeshima Y: Impaired negative feedback suppression of bile acid synthesis in mice lacking betaKlotho. *J Clin Invest* 115: 2202-2208, 2005.
65. Ge MX, Shao RG and He HW: Advances in understanding the regulatory mechanism of cholesterol 7 α -hydroxylase. *Biochem Pharmacol* 164: 152-164, 2019.
66. Samuel VT and Shulman GI: Mechanisms for insulin resistance: Common threads and missing links. *Cell* 148: 852-871, 2012.
67. Ye M, Sun J, Chen Y, Ren Q, Li Z, Zhao Y, Pan Y and Xue H: Oatmeal induced gut microbiota alteration and its relationship with improved lipid profiles: A secondary analysis of a randomized clinical trial. *Nutr Metab (Lond)* 17: 85, 2020.
68. Turnbaugh PJ, Ley RE, Mahowald MA, Magrini V, Mardis ER and Gordon JI: An obesity-associated gut microbiome with increased capacity for energy harvest. *Nature* 444: 1027-1031, 2006.



Copyright © 2024 Yang et al. This work is licensed under a Creative Commons Attribution-NonCommercial-NoDerivatives 4.0 International (CC BY-NC-ND 4.0) License.